Escola d'Enginyeria de Telecomunicació i Aeroespacial de Castelldefels
UNIVERSITAT POLITÈCNICA DE CATALUNYA

# TREBALL FINAL DE GRAU

**TÍTOL DEL TFG:** "THEORETICAL DESIGN OF A MAGNETIC ACTUATOR FOR NANOSATELLITE ATTITUDE CONTROL"

**TITULACIÓ:** Grau en Enginyeria de Sistemes Aeroespacials

**AUTOR:** Juan Francisco Lopera Zafra

**DIRECTOR:** Hyuk Park

**DATA:** 27 d'agost del 2019

**TÍTOL DEL TFG:** “THEORETICAL DESIGN OF A MAGNETIC ACTUATOR FOR NANOSATELLITE ATTITUDE CONTROL”

**TITULACIÓ:** Grau en Enginyeria d’Aeronavegació

**AUTOR:** Juan Francisco Lopera Zafra

**DIRECTOR:** Hyuk Park

**DATA:** 27 d’agost del 2019

**Resum**

Aquest treball presenta el disseny conceptual d’un actuador magnètic per a nano-satèl·lits, en específic per a CubeSats d’una unitat (1U, dimensions de 10 x 10 x 10 cm). Degut a les restriccions de mida d’aquest tipus de satèl·lit sovint es requereix dissenyar els subsistemes específicament per una missió en concret. Tot i així, també existeixen empreses que venen components genèrics que poden implementar-se segons els requeriments de la missió.

L’objectiu d’aquest treball és obtenir un disseny de magnetorquer que pugui ser implementat en futures missions amb CubeSats. A la primera part del treball es fa una introducció dels actuadors magnètics i s’expliquen els conceptes fonamentals sobre magnetisme.

Durant la fase de disseny s’explica en detall els models utilitzats, els paràmetres a tenir en compte durant el disseny de les bobines i la elecció i justificació dels valors escollits. També es tenen en compte les variacions típiques de temperatura en òrbites de baixa altura (LEO) per assegurar el correcte funcionament del sistema dins de les restriccions de consum de potència definides.

La solució obtinguda es testeja en un simulador ADCS dissenyat per la futura missió $^{3}$Cat-4 de la UPC. L’objectiu d’aquestes simulacions és demostrar que el disseny és capaç de generar el necessari moment magnètic com per controlar correctament una missió real. $^{3}$Cat-4 disposa de control magnètic i un “gravity boom” com a elements de control per tal de proporcionar precisió en l’orientació del satèl·lit.

Es demostra que la solució trobada ofereix el control desitjat en els eixos de roll i pitch en ambdues configuracions del “gravity boom” tot i l’efecte de les pertorbacions trobades en òrbites LEO.

**TITLE:** “THEORETICAL DESIGN OF A MAGNETIC ACTUATOR FOR NANOSATELLITE ATTITUDE CONTROL”

**AUTHOR:** Juan Francisco Lopera Zafra

**DIRECTOR:** Hyuk Park

**DATE:** 27th August 2019

**Overview**

This project presents the theoretical design of a magnetic actuator for use in nanosatellites, more precisely in 1U CubeSats (dimensions of 10 x 10 x 10 cm). The size restrictions found in this type of satellite usually require to design subsystems specifically for a mission. However, there also exist companies that sell generic components that can be implemented according to the specifications of the mission.

The aim of this work is to reach a magnetorquer design that can be used in future UPC CubeSat missions. The first part of this document introduces the fundamentals of magnetic actuators and magnetism.

In the design phase are presented the different used models, the parameters that need to be taken into account for the coils and core design and the discussion of the chosen values. Typical temperature variations in Low Earth Orbit (LEO) are also taken into account to ensure the performance of the system despite the defined power constraints.

The obtained solution is tested in an ADCS simulator designed for the future $^{3}$Cat-4 mission of the UPC. Simulations are performed to demonstrate that the design is able to generate the necessary magnetic moment and accurately control a real mission. $^{3}$Cat-4 makes use of magnetic actuators and a gravity boom as active and passive control components respectively in order to provide satellite pointing accuracy.

It is shown that the found solution provides the necessary control on roll and pitch angles for both configurations of the gravity boom, despite the effect of disturbances typically found in LEO orbits.

# INDEX

# CHAPTER 1. INTRODUCTION

Space exploration has become more accessible during the last decade due to the appearance of nanosatellites. Their reduction in size and mass compared to a conventional satellite not only drops drastically the cost of the mission but allows to deploy multiple missions per launch. This decrease in cost has caught the attention of many research centers interested in flying their own missions for educational and investigation purposes as well as companies that want to center their business model in offering space services.

One of the most important contributors in the increase of space accessibility was the definition of the CubeSat standard. CubeSats are satellites whose size is measured in multiples of 1U, i.e. 10 cm x 10 cm x 10cm. Its fixed dimensions and versatility has raised its popularity during the last years, since the standard offers enough margin for designers to be able to plan many different types of mission.

The definition of the standard also allows to design subsystems nonspecifically for a certain mission. There exist companies dedicated to manufacturing generic subsystems for CubeSats [1]. However, research centers and universities typically use self-made subsystems with the objective of reducing costs and allowing students to acquire knowledge and experience in the design processes of a mission which they can use in their future careers.

This work is focused in the theoretical design of a magnetorquer actuator for future CubeSat missions. The aim is to obtain a solution capable of providing accurate attitude control while also having as small dimensions as possible.

The solution is then tested in an ADCS (Attitude Determination and Control System) simulator developed for the $^{3}$Cat-4 mission from NanoSat Lab. The mission satellite is a 1U CubeSat with a gravity boom for passive control. Simulations are performed in LEO orbits to demonstrate that the magnetorquer design is capable to provide the magnetic moment required to accurately control the satellite in both gravity boom configurations despite the disturbances of aerodynamic drag, solar radiation pressure, gravity gradient and residual magnetic torques.

Chapter 1 provides theoretical knowledge about magnetorquers and their principle of operation, fundamentals of magnetic materials and a brief context about the CubeSat standard. Chapter 2 develops the design process of the magnetorquer and provides the results of the performed simulations. Conclusions of this work are given in Chapter 3.

# CHAPTER 2. THEORETICAL BACKGROUND

## 1.1. Magnetorquer principles

A magnetorquer, or magnetic torquer, is an attitude control system that makes use of the existing magnetic field on orbit in order to change the orientation of the satellite. The desired change of attitude is achieved by using a magnetic torque to rotate the satellite around its gravity center. This magnetic torque is the result of the interaction between the magnetic dipole generated by the magnetorquer and the available magnetic field on orbit (for example, Earth's magnetic field in LEO). Such interaction is expressed by the formula:

$$\boldsymbol{\tau} = \boldsymbol{m} \times \boldsymbol{B} \tag{1.1}$$

Where $\boldsymbol{\tau}$ is the resulting magnetic torque vector in [N·m], $\mathbf{m}$ is the magnetic dipole moment vector generated by the magnetorquer in [A·m$^2$] and $\mathbf{B}$ is the ambient magnetic field vector in [T] or [Wb/m$^2$].

According to equation (1.1), the generated torque is perpendicular to both the magnetic dipole moment and the magnetic field. The sense of the torque vector is such that the magnetic dipole (and, consequently, the satellite) tends to align to the magnetic field as a result.

The magnitude of the torque vector depends on the magnitude of both the magnetic dipole and the magnetic field vectors, and their orientation respect to each other. When $\mathbf{m}$ and $\mathbf{B}$ are orthogonal, the resulting torque is maximum. If both vectors are aligned, there is no applied torque.

A magnetorquer is usually formed by a set of three electromagnets. These coils are typically positioned so they are aligned with the body axis, orthogonal to and separate from each other, in order to simplify control implementation and avoid cross-coupling [2]. Some specific applications where magnetic torques are not the main source of control may opt for configurations of two or even one coil instead of a set of three.

The magnetic dipole moment generated by the system can be controlled by varying the current flow that passes through each coil. This is done by the Attitude Determination and Control System (ADCS), usually by switching on and off the coils according to the measured value of the magnetic field. More sophisticated implementations may use a proportional control manner by means of PWM signals or an I$^2$C interface to control the magnetorquer [3] [4].

Magnetorquers present several advantages that make them suitable for nanosatellite implementation. These include their low mass and power consumption, high energy efficiency and reliability, and an easy construction due to the lack of moving parts. Moreover, they do not need use of propellant, so they can virtually work forever providing there is enough electrical power available.

On the other hand, their dependence to an external magnetic field limits their utility up until geostationary altitude, since the strength of the Earth's field reduces with altitude. Thus the obtained torques are relatively weak and may need several orbits to decelerate enough the satellite. Moreover, uncertainty in magnetic models and errors in the measurements of Earth's field can lead to unstable control [5].

The major disadvantage of magnetorquers is their inability to produce a torque along the direction of the magnetic field, even if all three coils are used. This is so because the magnetic dipole cannot generate a torque if it is already aligned with the external field (see equation (1.1)). In polar orbits this issue has little effect because the direction of the field changes around the orbit, so the desired attitude can always be achieved at some point in orbit. However, in equatorial orbits the magnetic field is always oriented in the north-south direction, making magnetorquers not that useful for missions with such type of orbit.

For these reasons, magnetorquers are often used in the detumbling phase and tend to be combined with other types of control, such as aerodynamic or gravity-gradient torques. They are also used to counter environmental disturbance torques or to compensate for residual magnetic biases of the satellite [6].

There are three main types of magnetorquer currently being used in nanosatellites:

- Air-core magnetorquer: The simplest design of a magnetorquer, consisting in a conductive wire winded in a conveniently chosen number of circles and anchored to the satellite. They can provide a consistent magnetic dipole and are relatively light.

- Torquerod: It follows the same principle as the air-core, but in this case a bar or rod (the core) made of a magnetic material is surrounded by the wire, which is winded as a solenoid. This is the most efficient type of magnetorquer, as the core generates a higher dipole when excited by the coil. However, the magnetization curve of the core is not linear and presents hysteresis, and the material also keeps a residual magnetic dipole that does not disappear when the coil is switch off (remanence). The high increase in mass is also a critical disadvantage.

- Embedded coil: The coil is constructed on the PCB design in the form of copper traces. It is typically integrated in the solar panel, which relates to less volume used inside the satellite. On the other hand, the board thickness and the presence of the solar panel electronics limits the value of the magnetic dipole.

### 1.1.1 Magnetic coils

Magnetorquers make use of electromagnets, i.e. magnetic coils, to generate magnetic dipole moments for attitude and angular momentum control [6]. A *magnetic moment,* $\mathbf{m}$, is obtained when a single, plane wire loop is given an electrical current $\mathrm{I}$. This magnetic moment is proportional to both the current $\mathrm{I}$ and the area that encloses the wire loop $\mathrm{A}$:

$$\boldsymbol{m} = I \cdot A\, \hat{\boldsymbol{n}} \tag{1.2}$$

where $\hat{\boldsymbol{n}}$ is a unit vector normal to the plane of the loop and which sense is chosen according to the right-hand rule. For a group of $\mathrm{N}$ loops (or a coil of $\mathrm{N}$ turns) the contribution of all the turns can be summed up using the principle of superposition:

$$\boldsymbol{m} = N \cdot I \cdot A\, \hat{\boldsymbol{n}} \tag{1.3}$$

Given the relationship between the magnetic moment and the resulting torque of the magnetorquer in equation (1.1), it is of interest to maximize the magnetic moment produced by the coils. This is achieved by either increasing the number of turns of the coil, the consumed current or the area enclosed by each turn.

The magnetic effect of the solenoids is greatly affected by the material placed inside of them. If a *core* of a chosen material is inserted into the coil, the generated magnetic field may vary according to the magnetic properties of the material.

The selection of a proper material for the core is the most important parameter in the design of the magnetorquer. For example, cores made of ferromagnetic materials amplify the magnetic effects of the solenoid, which means that the same value of magnetic moment can be reached with less consumed power. On the other hand, these materials increase substantially the mass of the system and present several characteristics that make difficult to predict their behavior.

## 1.2 Fundamentals of Magnetism

Magnetism is a physical phenomenon by which certain objects perceive forces of attraction or repulsion towards another material. These forces originate from the interaction between magnetic fields and are dependent on their strength and orientation.

At atomic level, the magnetic field of a material is caused by its elementary particles, mainly its electrons. Electrons, as it is known, are charged particles that orbit around the nucleus of the atom, behaving like tiny current loops.

Moreover, they also spin along a certain axis according to their electron configuration. These two motions cause the electron to acquire a magnetic dipole moment, which makes it act as a tiny magnet.

The *net magnetic moment* of an atom is obtained by summing the contribution of both orbital and spin magnetic moments of all its electrons. However, in most materials these contributions tend to cancel each other. This is due to the electron configuration of the atom. On one hand, couples of electrons which share the same orbital have opposite spin magnetic moments, so their contribution is cancelled out. On the other hand, when an atom has a completely filled electron shell or subshell, then there is total cancellation of the orbital and spin moments of those electrons. This is the reason why some materials such as noble gases cannot be permanently magnetized.

### 1.2.1 H-field and B-field of a coil. Permeability of a material

A magnetic field is generated in the proximity of a conductive material when it is crossed by an electric current. An electromagnet generates a magnetic field whenever an electric current is supplied, and immediately ceases it when the current is turned off. The strength of the magnetic field generated is proportional to the amount of current through the electromagnet as seen in equation (1.3). This allows to control the magnetic field of the electromagnet as long as a continuous supply of current can be sustained.

The magnitude and direction of the generated field also depend on the geometry of the conductive material. Typically electromagnets take the form of a coil or solenoid because it concentrates the generated field into a nearly uniform field inside the solenoid [7] **(Fig. 1.1)**. The magnetic strength $\mathbf{H}$ of the coil is expressed by the formula:

$$H = \frac{NI}{l} \qquad \textbf{(1.4)}$$

where $\mathrm{N}$ is the number of turns, $\mathrm{I}$ is the current intensity in [A] and $\mathrm{l}$ the length of the coil. The unit of the magnetic strength $\mathbf{H}$ is [A/m].

From the previous expression can be observed that in order to increase the magnetic field of a coil one can either increase the number of turns or the current intensity, as well as try to reduce the distance between wire turns. The equation is an approximation of the real field generated and is only accurate in the inner region of the coil, far from its extremes.

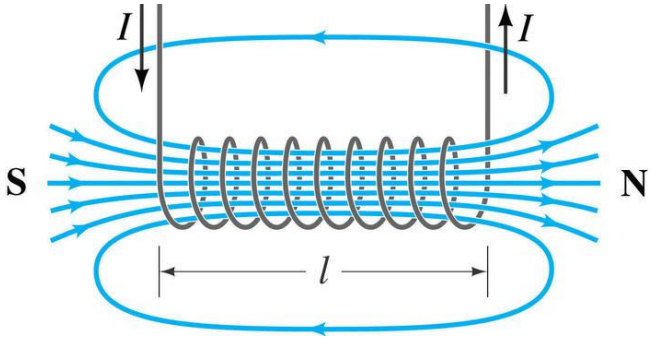


**Fig. 1.1** Magnetic field generated by a conductive wire in the shape of a coil. The field is divergent outside the coil, whereas it becomes a nearly uniform field on the inside.

The H-field is the consequence of exciting the solenoid with an electrical current. However, it does not take into account the influence of the medium in which the magnetic field is generated. The magnetic field of an electromagnet will have a different magnitude depending on the material of its core. The magnetic flux density, denoted as $\mathbf{B}$, represents the magnitude of the field generated in a substance or medium when it is subjected to an H-field. In a non-magnetized substance:

$$B = \mu \cdot H = \mu \frac{NI}{l} \tag{1.5}$$

where μ is the permeability of the material or medium through which $\mathbf{H}$ passes. Permeability of a material measures the degree of non-permanent magnetization that such material obtains in response to an applied magnetic field. It is measured in [H/m] or [N/A$^2$]. When the coil has an "air core", i.e. the medium is vacuum or air, μ takes a value of $\mu_0 = 4\pi \times 10^{-7}\ N/A^2$.

$\mu_0$ is called permeability of free space, and it is a constant value. For this reason, the permeability of a material $\mu$ is commonly expressed relative to $\mu_0$ rather than in absolute value:

$$\mu_r = \frac{\mu}{\mu_0} \tag{1.6}$$

If equation (1.5) is rearranged, $\mu$ can be expressed in terms of $\mathbf{B}$ and $\mathbf{H}$:

$$\mu = \frac{B}{H} \tag{1.7}$$

This expression is useful to obtain the permeability of a material by applying a known H-field to it and measuring the resulting B-field. Usually several

measurements for different values of $\mathbf{H}$ are made and are presented in a plot graph, with $\mathbf{B}$ in the vertical axis and $\mathbf{H}$ in the horizontal axis. The value of $\mu$ of a material is the slope of the plotted line **(Fig. 1.2)**.

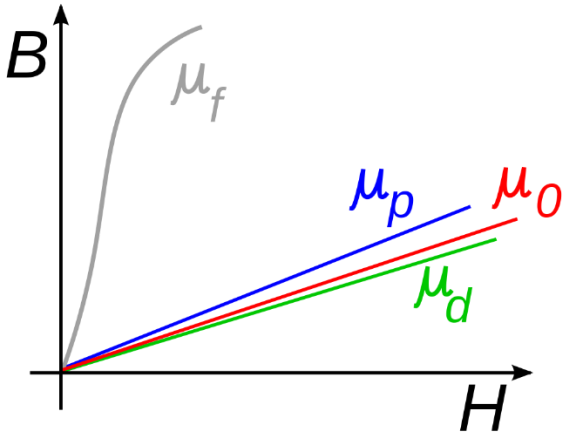


**Fig. 1.2** Simplified B vs. H plot comparing the permeability of different core materials: ferromagnetic ($\mu_f$), paramagnetic ($\mu_p$), free space ($\mu_0$) and diamagnetic ($\mu_d$).

*Note:* In literature, $\mathbf{H}$ and $\mathbf{B}$ are referred by many names. $\mathbf{H}$ is usually known as *magnetic strength*, *magnetic field intensity*, *H-field*, *magnetizing force*, *auxiliary magnetic field* or simply *magnetic field*. $\mathbf{B}$ is known as *magnetic flux density*, magnetic induction, B-field or simply magnetic field. The term *magnetic field* is usually used when it is clear which of the two fields ($\mathbf{H}$ or $\mathbf{B}$) is referred to.

### 1.2.2 Magnetization. Magnetic susceptibility

As it is known, certain materials are able to create a permanent magnetic field without the need of an electric current supply. The origin of this permanent magnetization comes from the orbital configuration of their atoms, which provides them with a net magnetic moment. When the magnetic moment of enough atoms point in the same direction their contributions are summed up and perceived macroscopically as a magnetic field.

Magnetization $\mathbf{M}$ is the vector field that expresses the density of, either permanent or induced, dipolar magnetic moments of a material [8]. It is defined as:

$$\boldsymbol{M} = \frac{d\boldsymbol{m}}{dV} \qquad \textbf{(1.8)}$$

where $\mathrm{d}\mathbf{m}$ is an infinitesimal element of dipolar magnetic moment, and $\mathrm{dV}$ is an infinitesimal element of volume. $\mathbf{M}$ is expressed in [A/m].

$\mathbf{M}$ can be understood as the amount of the dipolar magnetic moment per volume unit of medium. Rearranging the previous expression and integrating it is obtained:

$$\boldsymbol{m} = \iiint \boldsymbol{M}\, dV \tag{1.9}$$

where $\mathbf{m}$ is the dipolar magnetic moment of the medium. So, $\mathbf{m}$ can be determined by knowing the magnetization of the material. If $\mathbf{M}$ is uniform in the material then the integral can be simplified:

$$\boldsymbol{m} = \boldsymbol{M} \cdot V \tag{1.10}$$

However, magnetization is usually not given by manufacturers in commercially available magnetic material. Instead, the residual flux density (also known as remanence or retentivity) is given. In this case, $\mathbf{m}$ can be calculated as:

$$\boldsymbol{m} = \frac{1}{\mu_0}\boldsymbol{B}_r V \tag{1.11}$$

where $\mathbf{B}_r$ is the residual flux density, in [T].

Magnetization describes how a material responds to an external magnetic field, and how the field is altered by the presence of the material. If a magnetized core is introduced in a solenoid, the magnetic flux density $\mathbf{B}$ changes due to the influence of the magnetic field of the material:

$$\boldsymbol{B} = \mu_0(\boldsymbol{H} + \boldsymbol{M}) = \mu_0\boldsymbol{H} + \mu_0\boldsymbol{M} \tag{1.12}$$

So, the B-field is result of the superposition of the H-field and the magnetization of the core **(Fig. 1.3)**. In the case of a permanent magnet without induced field, the H-field inside the material is zero and there is only contribution of the magnetization of the material **(Fig. 1.4a)**. The complementary case is already discussed, i.e., an air-core coil supplied with an electrical current (See **Section 1.2.1**). In this case the magnetization $\mathbf{M}$ is zero in the entire region and the magnetic field inside the coil is proportional to the H-field as expressed by equation (1.5) **(Fig. 1.4b)** [8].

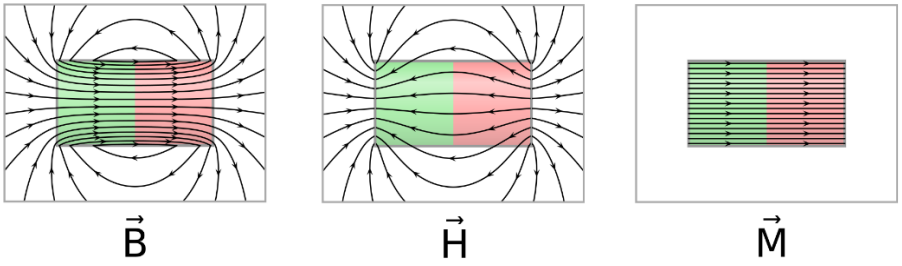


**Fig. 1.3** Fields $\mathbf{B}$, $\mathbf{H}$ and $\mathbf{M}$ of a magnetized cylinder. The B-field is proportional to the superposition of the H-field and the magnetization of the sample. Color red represents the North pole, color green represents the South pole. [9]

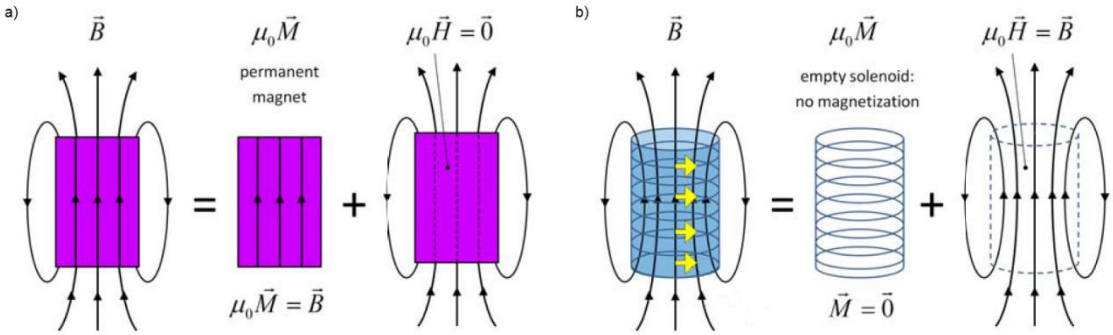


**Fig. 1.4 a)** The magnetic field produced by a permanent magnet is proportional to $\mathbf{M}$. **b)** In an air-core coil the magnetization is zero, and $\mathbf{B}$ is proportional to the H-field. [8]

In many materials there exists a relationship between $\mathbf{M}$ and $\mathbf{H}$. This relation depends on the type of material (see **Section 1.2.3**). In diamagnetic and paramagnetic materials, this relationship is lineal:

$$\boldsymbol{M} = \chi_m \boldsymbol{H} \tag{1.13}$$

where $\chi_m$ is known as volume magnetic susceptibility, and is a dimensionless quantity. Using this expression in equation (1.12) it is obtained:

$$\boldsymbol{B} = \mu_0(1+\chi_m)\boldsymbol{H} \tag{1.14}$$

and using equations (1.6) and (1.7) the relationship between volume magnetic susceptibility and relative permeability is found:

$$\mu = \mu_0(1+\chi_m) \tag{1.15}$$

$$(1 + \chi_m) = \frac{\mu}{\mu_0} = \mu_r \quad \textbf{(1.16)}$$

This expression is correct for diamagnetic and paramagnetic materials. However, it is invalid for ferromagnetic materials since the relation between $\mathbf{M}$ and $\mathbf{H}$ is not linear in their case due to the effect of hysteresis (see **Section 1.2.5**).

Volume magnetic susceptibility is a useful value to predict the magnetic behavior of a material. In the end, the fundamental laws of magnetism cannot be completely explained with classical physics. Measuring $\chi_m$ allows to make accurate predictions of the magnetic properties of a material without entering in quantum mechanical details [10].

### 1.2.3 Types of magnetism

Materials can be classified according to their behavior in the presence of an external material field. Such behavior is strongly related to the electronic configuration and the internal structure of the material. Among the different magnetic categories, three of them are of special interest in magnetorquer design:

- Diamagnetism: diamagnetic materials oppose their magnetic moment to the applied magnetic field. The observed B-field in these materials is slightly less than the observed in free space conditions; for this reason they have constant relative permeability $\mu_r$ of value slightly less than 1. Diamagnetism appears in all types of material but it is usually negligible when coexists with other types of magnetism and can only be appreciated in purely diamagnetic materials.

- Paramagnetism: paramagnetic materials are slightly attracted to external magnetic fields. In the presence of an external field they create an induced field in the same orientation, increasing the magnetic flux density. This materials have a constant relative permeability $\mu_r$ of value slightly more than 1. The magnetic properties of the material are lost once the external field is removed.

  The behavior of these type of materials is due to the fact that the electronic configuration of their atoms have incomplete shells. Uncoupled electrons cannot compensate their magnetic moment and act like tiny magnets. In the presence of an external field the magnetic moment of the electrons align to the external field and generate a net attraction force. When the external field is removed the magnetic moment of the electrons does not have any more tendency to align and takes a random direction, so overall their magnetic moments compensate and the magnetization of the material disappears.

- Ferromagnetism: the magnetization of these materials is much higher than that of paramagnetic ones. It depends on the applied field $\mathbf{H}$ and persists when the external field is removed. For this reason their relative permeability is not constant and can reach values of the order of $10^6$. Their magnetic materials are not only due to the electronic configuration of their atoms, which is similar to a paramagnetic one, but also on their crystalline structure. More details about the characteristics of ferromagnetic materials are discussed in the following sections.

Paramagnetic and ferromagnetic materials are of interest to be used for electromagnet cores. Paramagnetic materials have a low magnetic permeability, but they are easy to implement because their properties do not change in the presence of external fields. Ferromagnetic materials have a great permeability but they present non-linear behavior when exposed to a magnetic field.

**(Fig. 1.2)** shows the typical form of $\mathrm{B}$ vs. $\mathrm{H}$ plots for diamagnetic, paramagnetic and ferromagnetic materials. The order of magnitude of their permeability can be compared to the value for free space.

### 1.2.4 Demagnetizing field and demagnetizing factor

The magnetic behavior of a sample does not depend only on its intrinsic properties, but also on their geometry and dimensions. The effects due to the geometry of the sample are called demagnetizing effects, as they usually tend to reduce magnetization. The demagnetizing field $\mathbf{H}_\mathrm{d}$ or stray field is a magnetic field generated by the surface and volume magnetic pole densities of the sample in the opposite direction to the external field [11]. When an external field $\mathbf{H}_\mathrm{a}$ is applied to the sample, the total H-field at any point in space is:

$$\boldsymbol{H} = \boldsymbol{H}_a + \boldsymbol{H}_d \qquad \textbf{(1.17)}$$

The applied H-field is reduced due to the presence of the magnetized sample. The average volume magnetization of a sample $\mathbf{M}_\mathrm{vol}$, which depends on the shape and dimensions of the material, is related to the demagnetizing field $\mathbf{H}_\mathrm{d}$ such that:

$$\boldsymbol{H}_d = -\boldsymbol{N}_d \boldsymbol{M}_{vol} \qquad \textbf{(1.18)}$$

where $\mathbf{N}_\mathrm{d}$ is the demagnetizing tensor. Note that the negative sign in the expression denotes the fact that the demagnetizing field opposes to the contribution of the magnetization.

In general, $\mathbf{H}_d$ and $\mathbf{M}_{vol}$ cannot be assumed to be parallel [11]. In specific conditions though, this requirement is met and the demagnetizing tensor can be reduced to a scalar quantity called demagnetizing factor, defined as:

$$N_d = -\frac{H_d}{M_{vol}} \quad \textbf{(1.19)}$$

The directions in which $\mathbf{H}_d$ and $\mathbf{M}_{vol}$ are parallel are called the principal directions of the sample. In these directions, $\mathbf{N}_d$ can be reduced to a scalar. Also, it can be useful to express the demagnetizing tensor in the basis of the principal directions since it becomes a diagonal tensor.

## 1.2.5 Particularities of ferromagnetic materials

The behavior of ferromagnetic materials is more complex compared to that of diamagnetic or paramagnetic materials. Similar to paramagnetism, their magnetic properties come from their uncoupled electrons, causing a net magnetic moment on the atom. However, these magnetic moments not only have tendency to align with an external field, but also tend to align with the magnetic moments of atoms in the vicinity in order to reach a low energy state. This behavior causes ferromagnetic materials to present several particularities that explain their high permeability and being capable of being permanently magnetized.

### *1.2.5.1 Magnetic domains*

As previously mentioned, magnetic moments make electrons and atoms behave like tiny magnets. Due to this effect, nearby atoms can align their magnetic moments and form regions of material called magnetic domains where atom spins point in the same direction. A microcrystalline grain of material is formed by several adjacent domains, each one with its own direction of magnetization. Domains are separated by regions called domain walls, where magnetization rotates from that of one domain to the adjacent one **(Fig. 1.5)** [12].

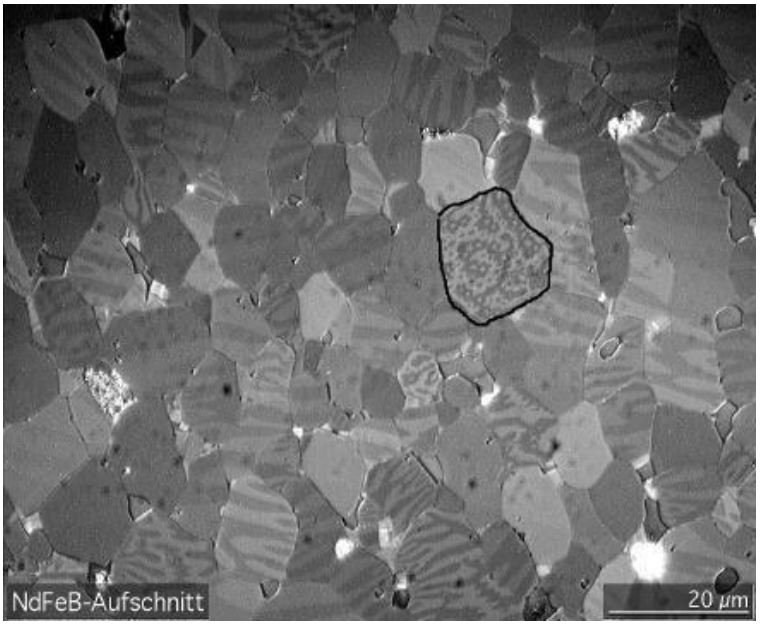


**Fig. 1.5** Microcrystalline grains in a piece of $Nd_2Fe_{14}B$ (alloy used in neodymium magnets). The domains are the light and dark stripes visible within each grain. In the outlined grain, the domains are aligned in the vertical axis, so the domains are seen end-on. [12]

The total magnetization of a sample is the sum of the magnetization of each one of the domains. In a non-magnetized sample each domain points in different random directions. This causes the magnetic moments to cancel out, so the total contribution of magnetization at macroscopic level tends to minimize.

*1.2.5.2 Magnetized states*

Although magnetic dipoles of atoms in the same domain may be aligned, creating strong local magnetic fields, the domain orientation along the entire sample is such that tends to reduce the total magnetization, give that it is the minimum energy state of the material.

However, it is possible to change the domain orientation to align them on the same direction, overall magnetizing the material. A ferromagnetic material is magnetized when an external H-field is applied: the domain walls move, causing already aligned domains to grow and the not aligned to reduce **(Fig. 1.6)**. When the external field is remove, domain walls remain in their new position and the contribution of the oriented domains is that to form a macroscopic magnetic field.

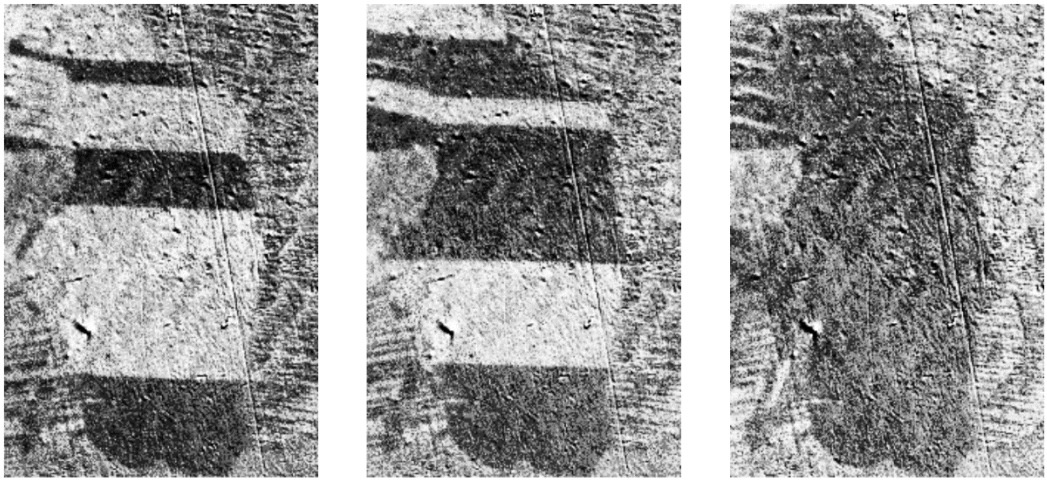

**Fig. 1.6** Domain walls moving due to an increasing external magnetic field. White areas are domains oriented upwards, dark domains are oriented down. [12]

As the H-field increases and more domains align to its direction, the generated B-field also increases. The relationship between $\mathbf{H}$ and $\mathbf{B}$ is not lineal **(Fig. 1.7)**: first $\mathbf{B}$ increases slowly and almost linearly for low values of $\mathbf{H}$, and then it increases faster as more domains align with $\mathbf{H}$. When the H-field reaches a certain value almost all the domains are aligned parallel to the external field. At this point, called the saturation limit, the magnetization has reached its maximum value and further increases of $\mathbf{B}$ are only due to the contribution of $\mathbf{H}$, linear and reversible.

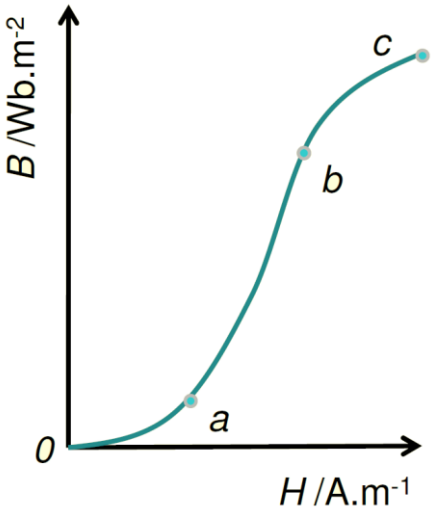


**Fig. 1.7** Plot $\mathbf{B}$ vs. $\mathbf{H}$ of a ferromagnetic sample. At $H$=0, the sample remains not magnetized. As $\mathbf{H}$ increases the domains switch their orientation to align with the H-field. From 0 to a, $\mathbf{B}$ increases almost linearly, so a constant value $\mu_i$ can be defined for this region. From a to b many domains are reorienting, thus the sample has a large value $\mu_r$. At point c the sample is saturated: its magnetization has reached its peak value and will not increase for higher values of $\mathbf{H}$. [13]

Since the relationship between $\mathbf{H}$ and $\mathbf{B}$ is not entirely linear, it is not possible to define a constant value of $\mu$ as with diamagnetic or paramagnetic materials. Instead, the value of the initial permeability $\mu_i$ for $H=0$ is usually used, since for low values of the H-field the variation of $\mathbf{B}$ can be considered as linear.

### *1.2.5.3 Hysteresis cycle*

Once the saturation limit is reached it can be assumed that all the domains of the sample are oriented according to the H-field. When $\mathbf{H}$ starts to decrease only some domains lose their alignment with the external field. This means that $\mathbf{B}$ does not decrease according to the initial magnetization curve, but describes a hysteresis curve **(Fig. 1.8)**. When $\mathbf{H}$ returns to 0 a large part of the domains remain in their new orientation, so the sample conserves a residual magnetic flux density called remanence or retentivity. Remanence $B_r$ represents the permanent magnetization of the magnetic sample.

If $\mathbf{H}$ increases again but in the opposite direction, the domains start to align according to the new orientation of the field. When $\mathbf{H}$ reaches a certain intensity, the magnetization of the sample is cancelled out with the H-field. This value of $\mathbf{H}$ is called coercivity.

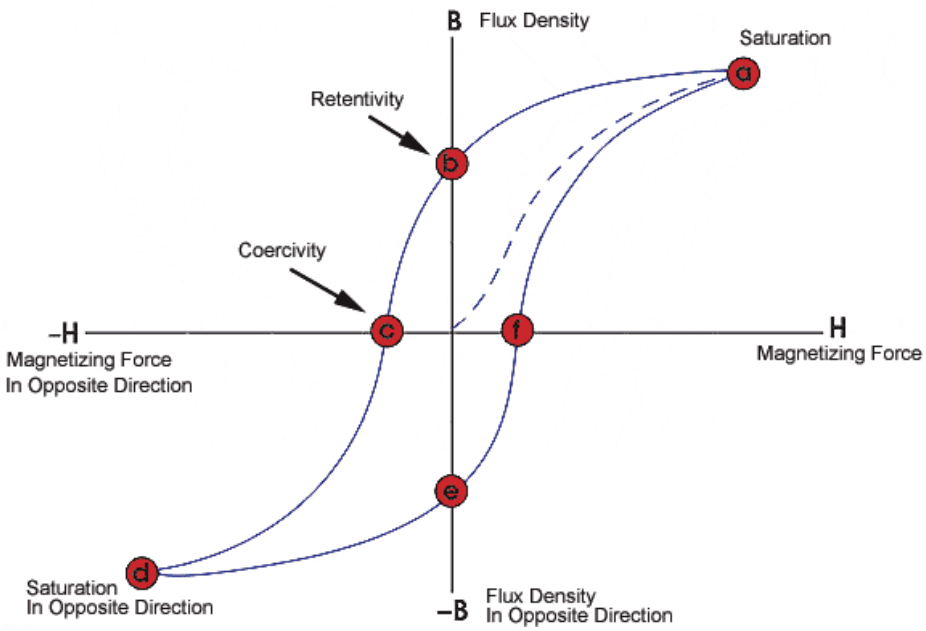


**Fig. 1.8** Representation of a hysteresis curve for a ferromagnetic material portraying the saturation points (a and d), retentivity points (b and e) and coercivity points (c and f). [14]

If $\mathbf{H}$ continues increasing the domains of the sample change their direction rapidly, eventually reaching the saturation limit. The magnetization of the material can be cycled around this loop over many field reversals [13].

The hysteresis cycle is characteristic of each material and varies in size and shape according to several factors. Given the atomic structure of the material and the direction of the applied field, the material may be easier or more difficult to magnetize than in other directions. This property is called magnetic anisotropy. Easier directions to magnetize present steeper hysteresis curves than other directions **(Fig. 1.9)**.

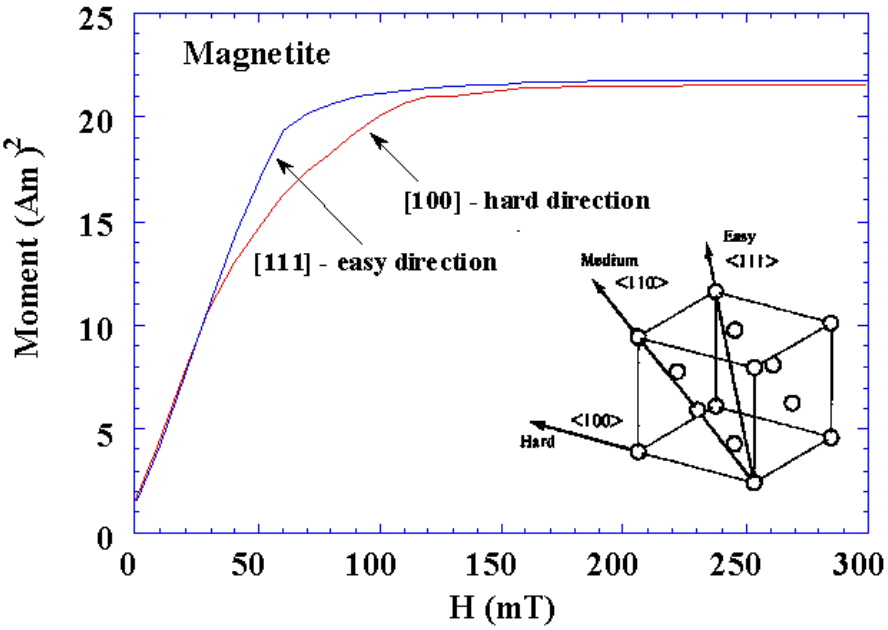


**Fig. 1.9** Plot **m** vs. **H** of a magnetite sample. The sample is magnetized in two different directions: [111] and [100]. The dipole moment in the first direction reaches the saturation limit for a lower value of H than the second direction. So, [111] is called an easy direction of magnetization and [100] a hard direction of magnetization. [15]

The area enclosed by the hysteresis loop is equivalent to the amount of energy loss per unit volume of material during a complete cycle [13]. According to the shape of the loop, ferromagnetic materials can be classified as soft or hard ferromagnetic **(Fig. 1.10)**. Soft ferromagnetic materials present a narrow hysteresis loop, which means a small energy loss per cycle. The narrow loop also implies a high permeability and low values of remanence and coercivity. For these reasons these materials are easy to demagnetize and usually reach the saturation limit with relatively low values of **H**. Soft ferromagnetic materials can be used in torquerods, as they can be magnetized and demagnetized with small magnetic fields that require low consumed power.

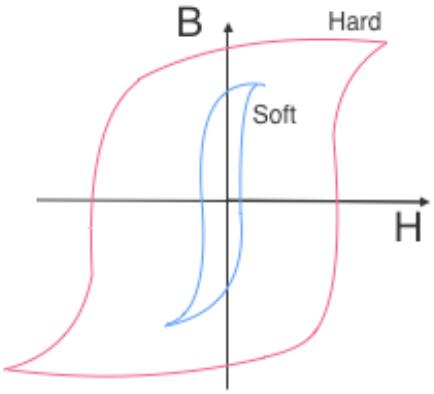


**Fig. 1.10** Schematic representation of the hysteresis cycle of a hard and soft ferromagnetic material. [16]

On the other hand, hard ferromagnetic materials have wider hysteresis loops and a low initial permeability, which means that they dissipate more energy per cycle and are more difficult to demagnetize. In order to reach the saturation limit they require a high H-field value, and present high remanence and coercivity. This materials are usually used as permanent magnets, for instance in nanosatellite passive control.

The frequency and waveform of the external H-field also affects the hysteresis cycle of the material. In general, the increase in frequency reduces the slope of the magnetization curve (and hence the permeability also is reduced) and increases the coercivity, the remanence and the energy loss [17] [18]. The waveform does not affect the shape of the hysteresis loop but has a little effect on coercivity and remanence [17].

#### *1.2.5.4 Degaussing*

Magnetization is not permanent. Magnetized samples remain in a high-energy state due to the alignment of the domains and, as many other systems in nature, will tend to a minimal-energy configuration, i.e., the demagnetized state. However, the magnetized state is metastable, which means that it is not the absolute minimum-energy state but a local one. For this reason, magnetization can persist for long periods of time, which may be a drawback depending on the application. For instance, magnetization of the torquerod of a satellite may alter the generated magnetic moment and disrupt the ACDS functioning.

There exist several methods for demagnetizing (also known as degaussing) a sample, the most effective being heating the material. Raising the temperature of the material increases the kinetic energy of the atoms, which causes their magnetic dipole moments to misalign. When the temperature reaches a certain value the orientation of the magnetic domains is no longer aligned but random, and the magnetization of the material is lost [13]. This value of temperature is called Curie temperature, and it is characteristic of each material. Ferromagnetic materials behave like paramagnetic when they are above their Curie temperature. When the material is cooled down it contains no residual

magnetic field, although the influence of Earth's magnetic field may magnetize the material again so it is convenient to be placed in an east-west orientation [19].

However, this process is not convenient for space application since Curie temperatures for typical ferromagnetic materials used in space are in the order of 500-1000 K and above. Instead, a common method used for demagnetizing a component is subjecting it to a reversing and decreasing magnetic field. The material proceeds to complete minor hysteresis cycles that collapse in a point where the magnetic dipoles return to a nearly random orientation, reaching an almost demagnetized state **(Fig. 1.11)**.

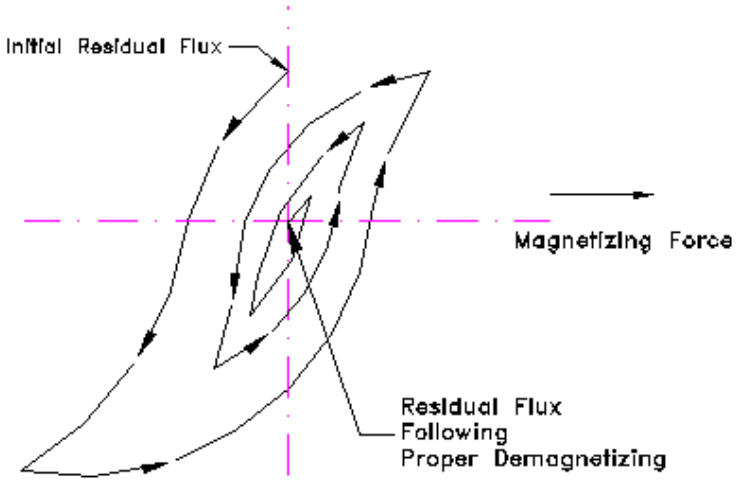


**Fig. 1.11** Successive hysteresis loops during the operation of demagnetizing a ferromagnetic sample. The loops collapse at a point near the origin. [20]

This method is used in satellite demagnetizing programs to demagnetize any material affected by the magnetic field of the magnetorquer, typically the core of the torquerods. A typical demagnetization program would take a few minutes [21]. Hard ferromagnetic materials are more difficult to demagnetize than soft ferromagnetic ones due to their wider hysteresis loops which implies more energy necessary to reach the demagnetized state.

## 1.3 The CubeSat Standard

CubeSat is a miniaturized satellite design standard developed by California Polytechnic State University (Cal Poly) and Stanford University. Its specification allow for the design, manufacture and launch of miniature satellites at an affordable cost and low development time, making it mainly appealing for universities interested in space research.

A CubeSat is formed by cubic units (U) of 10 cm x 10 cm x 10 cm and a maximum of 1.33 kg each [22]. This standard accomplishes several objectives.

The reduction in size also reduces the deployment cost, as several CubeSats can often be launched at once using the remaining capacity in launches of larger payloads. The unification of satellite sizes and shapes allows using a standardized platform for encapsulation and deployment (called P-POD, or Poly-PicoSatellite Orbital Deployer). This platform enables an easy integration to the launch vehicle and minimizes the risk of damaging it or other payloads.

Based on their mass, CubeSats typically belong to the picosatellite or nanosatellite categories of miniature satellites. They are often used in LEO missions, for experiments whose instruments can fit on them, such as for Remote Sensing. They can also be used for testing technologies with not enough reliability in the space sector at an affordable cost.

CubeSats have become really popular since 2013. As of January 2019, 1030 CubeSats have been launched [23]. Although they are mainly developed and launched for research and academic purposes, there are also companies interested in making profit out of the deployment and development of nanosatellites. For instance, PLD Space is currently developing a reusable launcher dedicated to small satellites which may be used in future ESA's missions [24].

Launch prices for CubeSats have been around $100.000 per cubic unit, although new operators are lowering the price to around $50.000 per cubic unit [25], which is also approximately its construct cost.

# CHAPTER 3. MAGNETORQUER DESIGN

This chapter describes the process followed during the design of a magnetorquer. First, the methodology used during this work is presented and discussed. Next, the design process is started by defining the requirements and constraints of the system, followed by the presentation of the models used, the presentation of several solutions and their discussion to choose a final solution. Finally, several simulations are performed using the $^{3}$Cat-4 mission [26] ADCS simulator to evaluate the performance of the solution on a real planned mission.

## 2.1 Engineering Design Process

The development of professional projects is often governed by a methodology frame which is stated before the project starts. Defining the process to follow beforehand helps to specify and schedule the required tasks to complete. A well-defined methodology also allows to estimate the necessary resources for the project such as money, time and human resources.

The Engineering Design Process is a series of steps that is typically followed by engineers to come up with a solution to a problem. Although there is no official or standard definition of the process, most of the variations follow similar steps **(Fig. 2.1).**

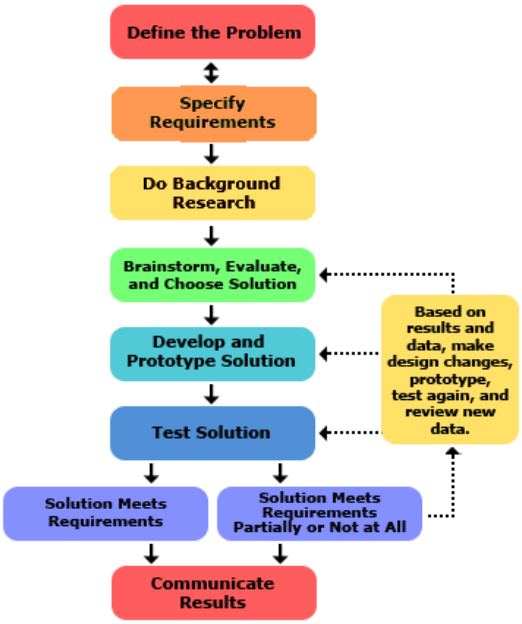


**Fig 2.1** Engineering Design Process steps.

The steps defined in the Engineering Design Process are:

- Define the problem or objective: The first step consists in specifying the problems that need to be solved. Often the client that needs the solution does not offer too much details or technical specifications of what they need. The purpose of this step is to collect all the available information in

order to clarify the objective of the design. Typical questions to solve in this step are: 'What is the problem or need?', 'Who has the problem?', 'What do we want to design?', 'Why is important to solve this problem?', etc.

- Identify the requirements and constraints: The final solution must meet several conditions in order to be valid for the given problem. On the other hand, there could be several restrictions that narrow the design window, such as a power, mass or economic budgets. An accurate specification of the requirements and constraints improves the design phase and helps to compare among possible solutions. A good way to identify design requirements is to analyse existing solutions and noting their key features.

- Background Research: Learning from previous solutions and asking others for their experiences helps to avoid previous mistakes and to know which technologies are adaptable to solve the problem.

- Brainstorm solutions and choose the best: At this point multiple solutions may seem appropriate to solve the problem. It is important to consider several solutions so as not to overlook a possible better one. Then, look at each possible solution and select the best one taking into account whether they meet all the requirements and how well they meet them.

- Develop the solution and build a prototype: During this step the design team can verify the performance of the solution and whether or not it works.

- Test and evaluate the solution: In this step the prototype is evaluated to confirm if it meets the requirements and is a proper solution to the problem. Analysis of what works and what can be improved is crucial, as well as communicating the solution with others to obtain feedback.

- Iterate: Based on the obtained results and feedback, the solution will meet the requirements completely, partially or even not at all. Using this data new requirements can be specified and changes can be made in the design. This step is crucial in the Engineering Design Process as it helps designers to learn from errors and improve the design until it meets the criteria given by the client.

- Communicate the results: When a good solution is reached, the final step consists in gathering all the information regarding the project into a final report, so that the solution can be understood, manufactured and supported by others.

## 2.2 Design objective and constraints

The aim of this thesis is to provide the conceptual design and specifications of a functional magnetic actuator that could be implemented in future CubeSat

missions. More precisely, the magnetorquer is aimed to be used for 1U CubeSats, which have a maximum cubic size of 1 $dm^3$ and 1.33 kg maximum mass.

One of the desired properties for the design is to be generic, i.e., not specific for a single mission. The proposed design should be able to be implemented in any type of LEO mission without modifying too much its original specifications. This requires that the performance of the system must be as high as possible considering general conditions for a typical mission. Contrary to bigger satellites which typically use components designed for a specific mission, CubeSat nanosatellite components are commercially available so customers just need to check for the necessary specifications. So, the CubeSat standard serves as a design boundary narrow enough for using manufactured subsystems not designed specifically for a certain mission.

The proposed solution must include a definition of all its key parameters: type of magnetorquer, wire material and width, coil radius, number of turns, core material, total mass and dimensions, consumed power and maximum generated dipole.

Reviewing similar commercially available systems and other designs from literature [1] [27] [28], several requirements and constraints are defined to obtain an optimal design **(Table 2.1).** The definition of these constraints seeks to reach a design that could fit in different types of mission, so feasible values have been selected for them. On the other hand, the minimum required magnetic dipole is easy to obtain with the given constraints. Ultimately this requirement is driven by the “as high as possible” principle.

| Constraints | Value | Requirements | Value |
|---|---|---|---|
| Voltage supply | 3.3 V or 5 V | Magnetic dipole moment | >0.07 $A \cdot m^2$ |
| Power loss | < 0.3 W (per coil) | | |
| Mass | < 0.03 kg (per coil) | | |

**Table 2.1** Constraints and requirements of the design.

## 2.3 Design process

This section describes the steps followed in the design process of a magnetorquer. As discussed in the previous section, it results of great interest to obtain a design that may be suitable for several types of mission. For this reason, it is important to consider the pros and cons of each type of magnetorquer coil in order to reach an adaptable solution.

The presented solution in this work is formed by an air core coil and two torquerods. Torquerods require big mass and dimension budget, but they are extremely efficient in energetic terms and generate a high magnetic moment. On the other hand, air core coils don’t produce such high amount of magnetic

moment but they are easy to implement in any king of mission due to their typical dimensions.

Embedded coils, although being interesting a priori because of being attached to solar cells which reduces the dimensions of the system, they require a thermal study which is more dependent on the characteristics of the rest of the satellite, and require the availability to be mounted on the faces of the CubeSat. For these reasons, embedded magnetorquer was discarded of the design process.

The design of the two types of coil is made taking into account the dimensions of a 1U CubeSat and considering having a smaller size system more than reaching the maximum amount of dipole possible.

### 2.3.1 Air core coil design

This section describes the design of the air core coil of the magnetorquer. In an attempt to show how the Engineering Design Process works, first several simple designs are presented and then improvements are applied to them in order to reach a better final solution.

As explained above, air core magnetorquers consist basically in a coil with no core in the inside. In this type of magnetorquer, equation (1.3) provides a good approximation of the behaviour of the coil. An optimal design of the magnetorquer requires the maximization of these parameters. $A$ is mainly limited by the dimensions of the CubeSat, whereas an increase in $N$ or $I$ will affect either the mass or the power consumption of the system. Therefore the relation between the resulting moment $m$ and the required mass and power must be studied.

Expressions for the mass and consumed power of the coil can be obtained by defining its characteristics. Considering the coil as an electrical conductor with constant cross section and uniformly distributed mass, the resistance of the wire $R$ can be defined in terms of the length $L$ and cross-sectional area $S$ of the wire as. Assuming the coil is made of circle turns:

$$R = \sigma \frac{L}{S} = \sigma \frac{2\pi r \cdot N}{S} \qquad \textbf{(2.1)}$$

where $r$ is the radius of one turn of the coil and $\sigma$ is the electrical resistivity of the material of the coil in [Ω·m]. This relation can be rearranged in terms of the number of turns:

$$N = \frac{RS}{2\pi r \sigma} \qquad \textbf{(2.2)}$$

Consumed power, intensity and resistance are interrelated by the following expression:

$$P = I^2 R \tag{2.3}$$

$$I = \sqrt{\frac{P}{R}} \tag{2.4}$$

On the other hand, the mass $\mathrm{M}$ of the coil can be computed by means of the volume of the wire and the density of the material:

$$M = \rho L S = \rho \cdot 2\pi r N \cdot S \tag{2.5}$$

in which again the number of turns can be isolated giving the expression:

$$N = \frac{M}{2\pi r S \rho} \tag{2.6}$$

Finally, equations (1.2), (2.2), (2.4) and (2.6) are combined to find the relationship between $\mathrm{m}$, $\mathrm{M}$ and $\mathrm{P}$:

$$m = NIA = N\sqrt{\frac{P}{R}}A = \sqrt{\frac{N^2 P}{R}}A = \sqrt{\left(\frac{RS}{2\pi r\sigma}\frac{M}{2\pi r S\rho}\frac{P}{R}\right)}\,\pi r^2 \tag{2.7}$$

$$m = \sqrt{\frac{PM}{\sigma\rho}} \cdot \frac{\pi r^2}{2\pi r} = \frac{r}{2}\sqrt{\frac{PM}{\sigma\rho}} \tag{2.8}$$

Last expression reflects several key points that need to be taken into account during the design process. First, the magnetic dipole increases linearly with the radius of the coil. This seems logical since it reflects the dependence of the magnetic moment to the area of the turns in equation (1.3). It results of interest to select a value of $\mathrm{r}$ as large as possible, considering the limitations given by the CubeSat Standard and the dimensions of the frame [22].

Second, it can be noticed that the number of turns does no longer appear in the expression. Power and mass appear multiplied, which implies that power consumption can be decreased by increasing the mass of the system and vice versa. This trade-off is adjusted by selecting the number of turns of the coil. For a fixed voltage and coil radius, an increase of $\mathrm{N}$ raises the mass of the system but also the resistance of the wire, which reduces the consumed power.

However, the obtained magnetic moment does not change according to the number of turns **(Fig. 2.2).**

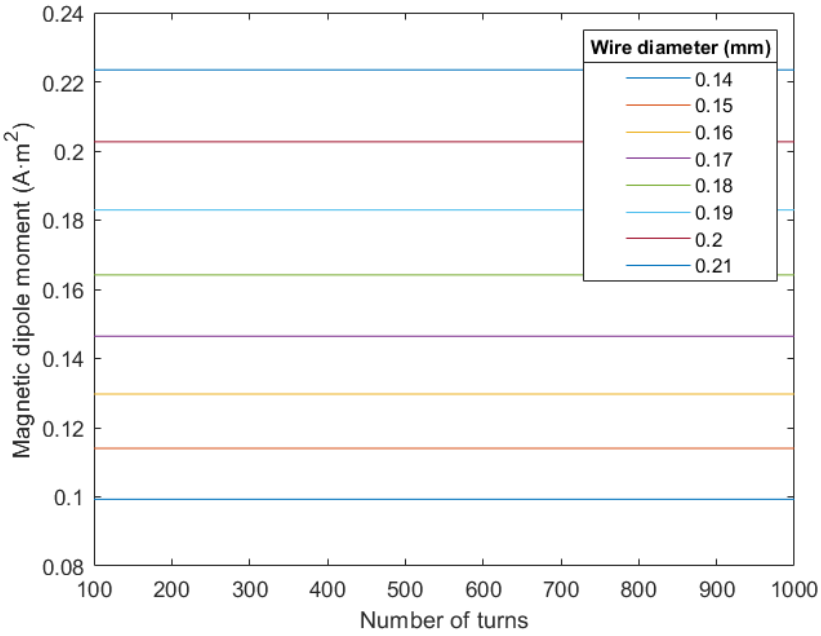


**Fig. 2.2** Magnetic moment vs. number of turns for different wire diameters (V= 5V, r= 40 mm). Large diameters increase the generated magnetic moment. The number of turns does not affect the magnetic moment for a fixed voltage, coil radius and wire diameter.

Power consumption and mass are also affected by the chosen wire diameter. A thicker wire increases both the mass and consumed power of the system, but also generates a larger magnetic moment as a result. The relationship between magnetic moment and wire diameter is not linear but quadratic **(Fig. 2.3)**.

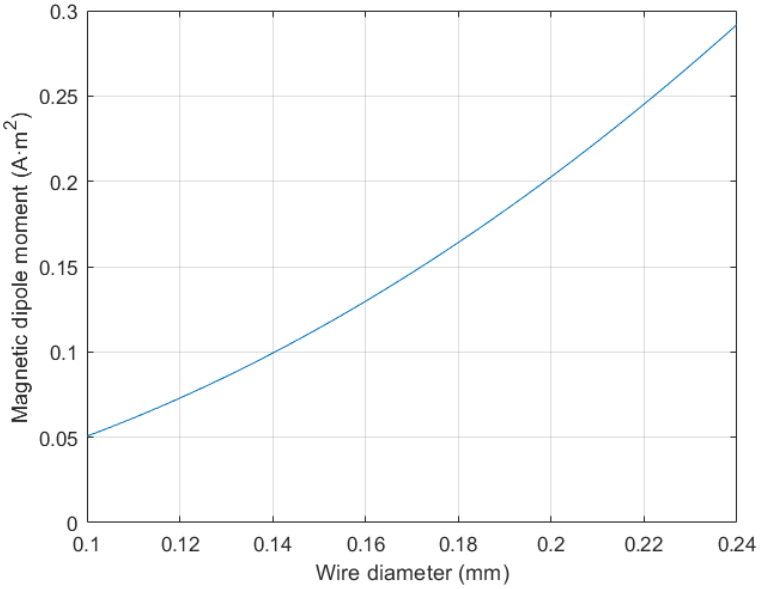


**Fig. 2.3** Magnetic moment vs. wire diameter.

Lastly, some intrinsic properties of the coil material also affect the magnitude of the generated dipole, mainly its density ($\rho$) and electrical resistivity ($\sigma$). The lower the product of these two properties is, the higher magnetic moment is generated and more torque is obtained for the same mass and power budgets. For this reason the selection of the proper material to manufacture the coil is crucial.

Typically used materials are copper and aluminium. Copper has lower electrical resistivity $\sigma$, whereas aluminium has lower $\sigma\rho$ product **(Table 2.2)**.

| | **Copper** | **Aluminium** |
|---|---|---|
| Density ρ [kg/m$^3$] | 8.93E+03 | 2.70E+03 |
| Electrical resistivity σ (at 20ºC) [Ω•m] | 1.55E-08 | 2.50E-08 |
| σ·ρ | 1.384E-04 | 0.675E-04 |
| Temperature coefficient of resistivity (at 20ºC) [1/K] | 3.90E-03 | 3.90E-03 |

**Table 2.2** Properties of interest of copper and aluminium. [28]

For example, using equation (2.8) to compare the magnetic moments of two identical coils but one made of copper and the other of aluminium it is seen that

$$\frac{m_{Al}}{m_{Cu}} = \sqrt{\frac{(\sigma\rho)_{Cu}}{(\sigma\rho)_{Al}}} = \sqrt{\frac{1.8 \cdot 10^{-4}}{0.8 \cdot 10^{-4}}} \cong 1.43$$

meaning that a coil made of Aluminium will provide a 43% higher torque approximately than a copper one under the same conditions.

In practice, choosing the right material does not depend that much on the produced torque but on whether the mass or the dimensions of the system are the main constraint of the design. The low density of the aluminium means that more volume is required for the same amount of mass respect to a copper coil. In this study, the desired dimensions of the system are more restrictive than the mass budget, so copper is used as the wire material.

Having all these considerations in mind, the design of the air core coil consists in selecting the wire diameter and number of turns that produce the maximum magnetic moment for the chosen material and coil radius while complying with the proposed constraints. **(Fig. 2.4)** and **(Fig. 2.5)** show the power consumption and mass of the coil depending on these two parameters, considering circle coils of 40 mm radius and a voltage supply of 5 V.

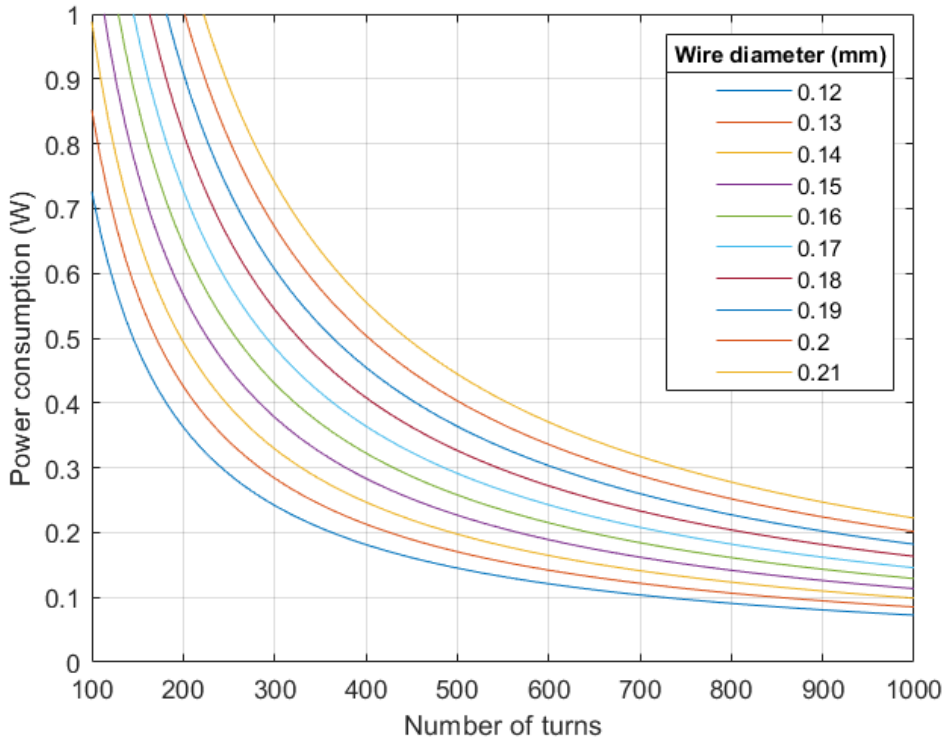


**Fig. 2.4** Power consumption model for several wire diameters and number of turns (circle coils, V= 5V, r= 40 mm).

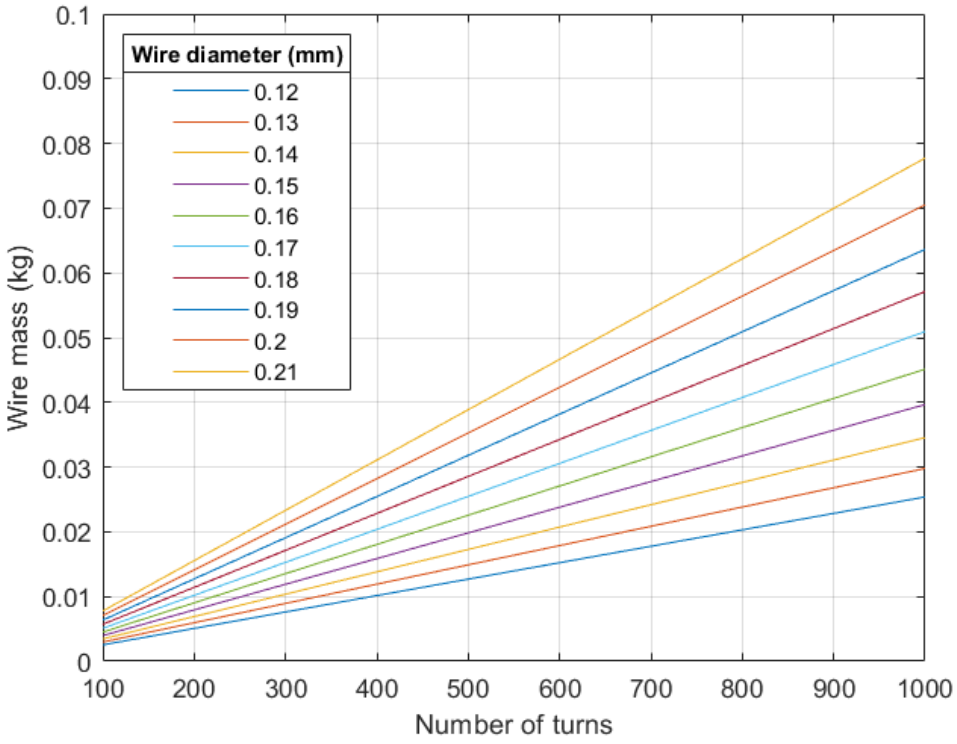


**Fig. 2.5** Coil mass model for several wire diameters and number of turns (circle coils, V= 5V, r= 40 mm).

Making use of these models one can choose possible coil designs which would provide a good compromise among the specified requirements and constraints. The proposed solutions and their characteristics are presented in **(Table 2.3)**.

| | V [V] | r [mm] | N [-] | a [mm] | $P_{max}$ [mW] | M [g] | $m_{max}$ [A·m$^2$] |
|---|---|---|---|---|---|---|---|
| Design 1 | 5 | 40 | 580 | 0.15 | 195.5 | 23.00 | 0.1140 |
| Design 2 | 5 | 40 | 600 | 0.16 | 215.1 | 27.08 | 0.1297 |
| Design 3 | 5 | 40 | 500 | 0.17 | 291.3 | 25.47 | 0.1464 |
| Design 4 | 5 | 40 | 580 | 0.17 | 251.1 | 29.55 | 0.1464 |

**Table 2.3** Possible designs of the air core with circle coils. Parameters: Voltage (V), coil radius (r), number of turns (N), wire diameter (a), maximum consumed power ($P_{max}$), wire mass (M) and maximum generated magnetic moment ($m_{max}$).

At least one design has been presented for each reasonable value of wire diameter. Design 1 has low values of power, mass and dipole, which indicates that resources may be underused. Designs 3 and 4 have more limited margin for improvement, and each one has been chosen valuing more mass and power respectively.

Once presented a first set of possible solutions, a second iteration of the process is made taking more variables into account in order to obtain better solutions.

For instance, the performance of different shapes for the coil turns may be studied. Due to the cubic shape of the satellite, it may seem reasonable to consider square turns instead of circle ones in order to make better use of the available space.

The ratio between the area A enclosed by a turn and the length of that wire L can be used to compare how much area is obtained per unit length of coil. A high A/L ratio means more area is obtained for the same amount of wire, effectively increasing the obtained dipole by just changing the shape of the coil.

Consider a circle turn and a square turn whose diameter and side are both equal to 2r. Their A/L ratios result to be the same, which means the same amount of area is obtained for the same amount of wire no matter which shape is chosen. Despite the square covers more area than the circle, it also requires more wire to do so. For the same length of wire, a circular coil will have more turns than a square one, but it will also cover less area per turn. As a result, the product N·A remains equal for both configurations, which means the same amount of dipole is obtained in both coils.

However, the fact that square turns use more wire than circle ones results convenient in the air core design. This allows to spread the coil in the radial direction instead of perpendicular to the plane of the turns. Moreover, shaping the coil with the form of the satellite also helps to fit it inside the frame and increase the coil dimensions.

The design of square coils in this work is made considering a side length of 90 mm ($r$=45 mm) and a voltage of 5 V, both values being realistic for a CubeSat mission. The same design process is followed for circle coils, but equations (2.1), (2.2), (2.5) and (2.6) now must be evaluated for $L=4\cdot(2r)$ and $A=(2r)^2$. As a result, expressions for mass and consumed power appear to be the same as for circle coils, but multiplied and divided by a factor of π/4 respectively. This means that a square coil approximately weighs a 21% more and consumes a 21% less power respect to a circle coil of the same dimensions, number of turns and wire diameter.

However, the expression for the magnetic dipole remains unchanged, reflecting that variations in mass and consumed power cancel out and coils of the same characteristics produce the same amount of magnetic moment, regardless of their shape.

**(Fig. 2.6)** and **(Fig. 2.7)** show the dependence of consumed power and mass for different number of turns and wire diameters in square coils, considering square coils of $r$=45 mm and a voltage supply of $V$=5 V.

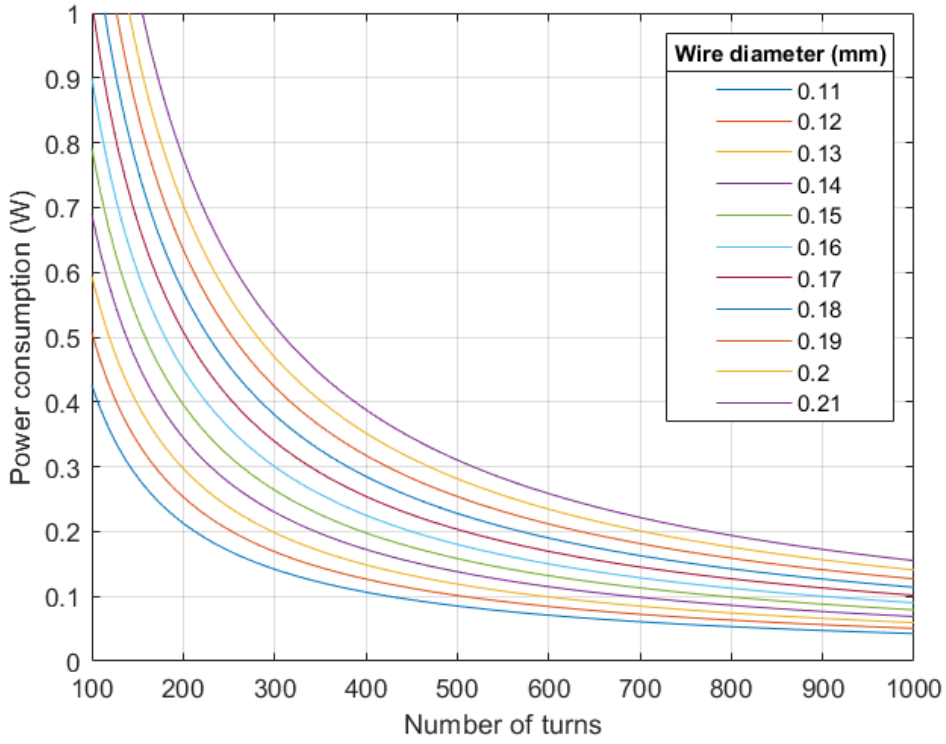


**Fig 2.6** Power consumption model for several wire diameters and number of turns (square coils, $V$= 5V, $r$= 45 mm).

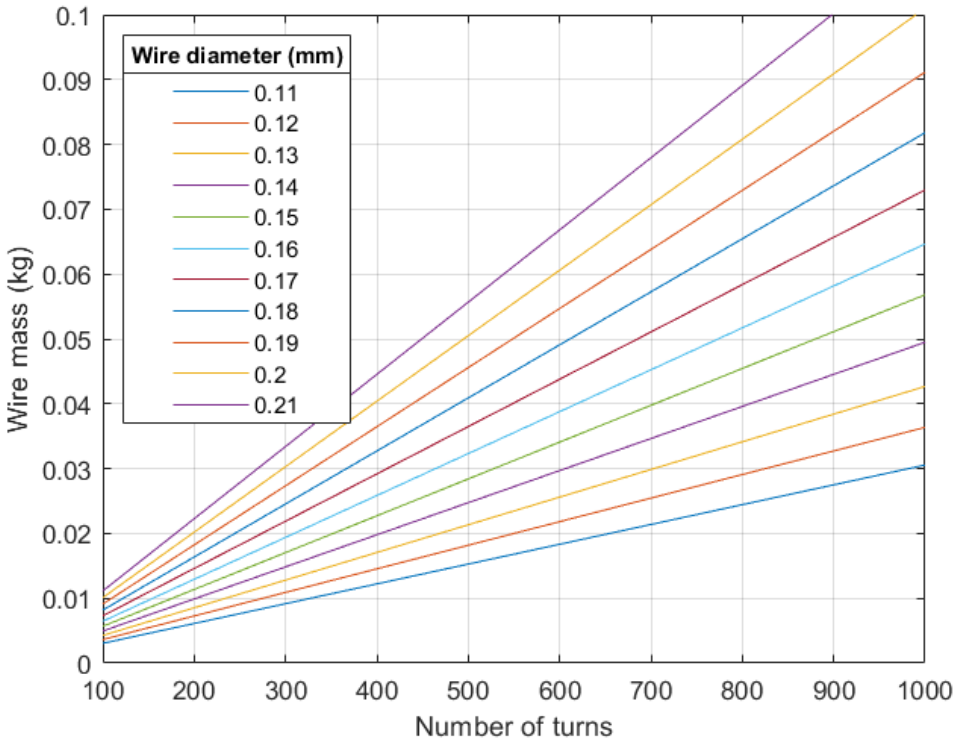


**Fig. 2.7** Coil mass model for several wire diameters and number of turns (square coils, V= 5V, r= 40 mm).

The following table presents several solutions using square coils for the air core magnetorquer **(Table 2.4)**. This set of solutions has been chosen valuing power more than mass in an attempt to reduce power consumption as much as possible.

| | V [V] | r [mm] | N [-] | a [mm] | $P_{max}$ [mW] | M [g] | $m_{max}$ [A·m$^2$] |
|---|---|---|---|---|---|---|---|
| Design 5 | 5 | 45 | 420 | 0.16 | 214.5 | 27.15 | 0.1459 |
| Design 6 | 5 | 45 | 460 | 0.16 | 195.8 | 29.73 | 0.1459 |
| Design 7 | 5 | 45 | 370 | 0.17 | 274.8 | 27.00 | 0.1647 |
| Design 8 | 5 | 45 | 390 | 0.17 | 260.8 | 28.45 | 0.1647 |
| Design 9 | 5 | 45 | 400 | 0.17 | 254.2 | 29.19 | 0.1647 |

**Table 2.4** Possible designs of the air core with square coils.

The values of magnetic dipole moment obtained for each solution are theoretical and obtained considering that each turn covers the exact same amount of area. In practice, the high number of turns causes that the wire diameter cannot be neglected, so the coil will either increase in the radial direction or orthogonal to it. Growing in the radial direction means wounding wire over the previous winding, so there will be changes in the area of the turns that will affect the generated dipole. These variations must be studied in order to consider them negligible or not.

Air core coils are typically wounded in supports which allow the coil to grow in the radial direction while limiting the growth in the direction of the coil axis to 3-4 mm in general. Fixing this dimension, the total growth in the radial direction can be modelled based on the number of turns of the coil and the wire diameter.

As already mentioned, coils are wounded so first it grows in the direction of its axis, and once the layer is completed the winding continues above the previous layer, hence increasing the area of the coil. In the presented model though, this procedure is considered backwards: first the turns are considered to have dimensions equal as the ones chosen in the design process, and once the layer is finished a new layer is started below the previous one. This is so because the desired dimensions are the maximum ones available for the system and turns that do not fit need to be smaller, which causes a reduction in the area turn and hence a reduction of the performance of the system.

Results of the applied model are shown in **(Fig. 2.8)**, considering a maximum thickness of the support of 4 mm and turns with $r$ =45 mm. For a wire diameter and number of turns a corrective factor is given that expresses the ratio between the effective and the real obtained magnetic dipoles. Increasing the wire diameter or the number of turns of the coil lowers the effective magnetic moment because more layers of wire are required to fit the coil around the support. The model does not change depending on the shape of the coil.

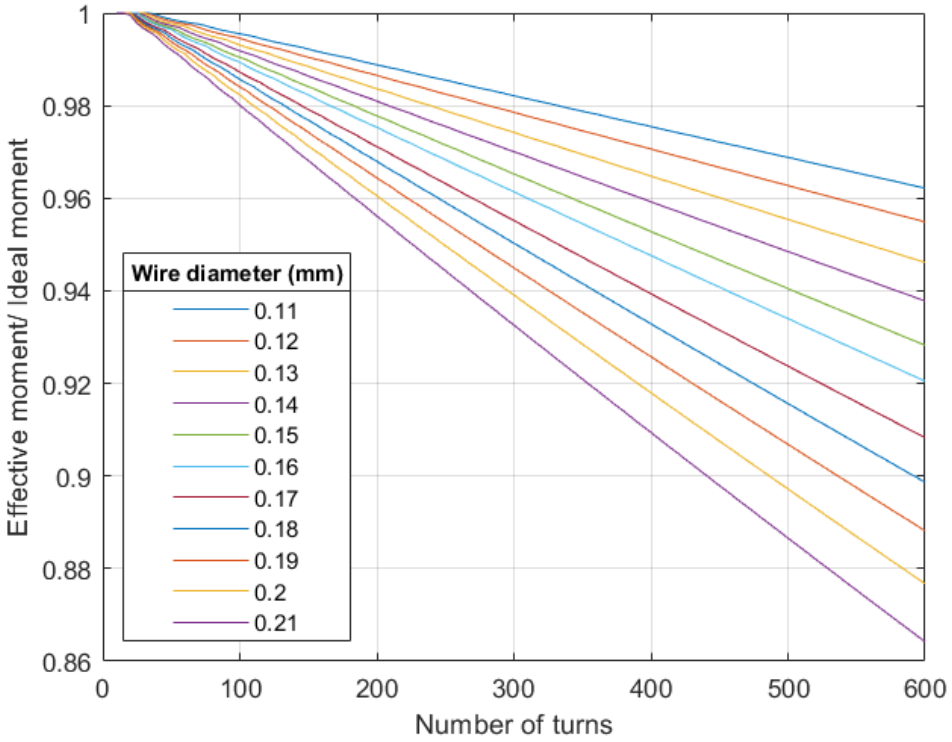


**Fig. 2.8** Reduction in the obtained dipole for coils of $r$=45 mm in a support with a thickness of 4 mm.

Another factor still not considered in the design process is the influence of large temperature variations on the behaviour of the coil along the orbit. These variations affect the resistance of the wire, which varies the expected consumed power and the generated magnetic moment.

The electrical resistivity σ of a material, which was assumed in equation (2.1) to be constant, depends on the temperature of the wire. For relatively low temperature variations, i.e. changes of several tens of degrees, the relation can be considered as lineal:

$$\sigma(T) = \sigma_0 \cdot [1 + \alpha_0 \cdot (T - T_0)] \quad \textbf{(2.9)}$$

In this expression, $\sigma_0$ is the value of electrical resistivity at a chosen temperature $T_0$ and $\alpha_0$ is called temperature coefficient of resistivity, which is an empirical parameter. **(Table 2.2)** shows their values at T=20 ºC for copper and aluminium.

Previous designs have been obtained considering a constant value of $\sigma$ at a temperature of 20 ºC. This is not a realistic assumption since temperature can present variations from -100 ºC to 100 ºC depending on the type of LEO orbit and the satellite thermal control. An accurate temperature range for a specific mission can be obtained performing a thermal control study, which is out of the scope of this work. Furthermore, the aim of the design is to find a solution suitable in different missions, so it is necessary to evaluate the designs within the mentioned temperature range.

To perform this task, power consumed and magnetic moment at different temperatures is computed taking into account the changes in their electrical resistivity. Wire resistance decreases with temperature, which increases power consumption. On the other hand, higher temperatures decrease power consumption, which also decreases the magnetic moment. A good design must be able to actuate within a temperature range considered acceptable with a reasonable amount of magnetic moment while complying with the given power constraints.

The following table shows power consumption and theoretical magnetic moment for each presented design at different temperatures **(Table 2.5)**. Power consumption has been evaluated for temperatures lower than 20ºC and theoretical magnetic moment for higher temperatures. It has been considered that a good design must comply with the magnetic dipole requirement for the entire temperature interval and without surpassing the maximum consumed power at least until reaching a temperature of -50ºC. Designs that do not meet this constraint will be discarded.

| | $P_{max}$ [mW] | | | | | $M_{max}$ [A·m$^2$] | | | |
|---|---|---|---|---|---|---|---|---|---|
| T [ºC] | 20 | -30 | -50 | -70 | -90 | 20 | 50 | 70 | 100 |
| Design 1 | 195.5 | 242.9 | 269.0 | 301.3 | 342.4 | 0.1140 | 0.1021 | 0.0954 | 0.0869 |
| Design 2 | 215.1 | 267.1 | 295.8 | 331.4 | 376.6 | 0.1297 | 0.1161 | 0.1086 | 0.0989 |
| Design 3 | 291.3 | 361.9 | 400.7 | 448.9 | 510.2 | 0.1464 | 0.1311 | 0.1225 | 0.1116 |
| Design 4 | 251.1 | 312.0 | 345.5 | 387.0 | 439.8 | 0.1464 | 0.1311 | 0.1225 | 0.1116 |
| Design 5 | 214.5 | 266.4 | 295.0 | 330.5 | 375.6 | 0.1459 | 0.1306 | 0.1221 | 0.1112 |
| Design 6 | 195.8 | 243.3 | 269.4 | 301.7 | 343.0 | 0.1459 | 0.1306 | 0.1221 | 0.1112 |
| Design 7 | 274.8 | 341.4 | 378.1 | 423.5 | 481.3 | 0.1647 | 0.1475 | 0.1379 | 0.1256 |
| Design 8 | 260.8 | 323.9 | 358.7 | 401.8 | 456.7 | 0.1647 | 0.1475 | 0.1379 | 0.1256 |
| Design 9 | 254.2 | 315.8 | 349.7 | 391.7 | 445.2 | 0.1647 | 0.1475 | 0.1379 | 0.1256 |

**Table 2.5** Power consumption and magnetic moment obtained at different for each proposed design. Values in red do not comply with the constraints of the design.

From these results it can be expected that designs 3, 4, 7, 8 and 9 would not comply with the power constraint with fully charged batteries even at a temperature of -30ºC and would require lower voltage to work. Reaching this temperature in orbit is not uncommon and the actuator should function in nominal conditions without limiting the voltage supplied to it. For this reason, they are discarded from the list of possible solutions. On the other hand, minimum magnetic dipole moment is reached for all solutions at any possible temperature, so no more designs need to be discarded regarding this requirement.

The final list of possible designs is presented in **(Table 2.6)**, including a summary of their most important characteristics. The selection of a final design must be performed comparing how much magnetic moment they can provide and how well they adjust to the given constraints.

| | Coil shape | V [V] | r [mm] | N [1] | a [mm] | $P_{max}$ (T=20ºC) [mW] | $P_{max}$ (T=-50ºC) [mW] | M [g] | $m_{max}$ (T=20ºC) [A·m$^2$] | $m_{eff}$ (T=20ºC) [A·m$^2$] |
|---|---|---|---|---|---|---|---|---|---|---|
| Design 1 | Round | 5 | 40 | 580 | 0.15 | 195.5 | 269.0 | 23.00 | 0.1140 | 0.1051 |
| Design 2 | Round | 5 | 40 | 600 | 0.16 | 215.1 | 295.8 | 27.08 | 0.1297 | 0.1181 |
| Design 5 | Square | 5 | 45 | 420 | 0.16 | 214.5 | 295.0 | 27.15 | 0.1459 | 0.1379 |
| Design 6 | Square | 5 | 45 | 460 | 0.16 | 195.8 | 269.4 | 29.73 | 0.1459 | 0.1371 |

**Table 2.6** Final list of fitting designs.

From data one can observe the effect of the dimensions and shape of the coil in the final magnetic moment. Square turns fit better into the satellite frame given that they have the same shape, which allows to enlarge the dimensions of the coil and generate a large magnetic moment. On the other hand, choosing the right wire diameter is key to find solutions that neither exceed the constraints

nor perform poorly compared to other designs. In this case, Designs 1 and 2 seem not to be the right choice for the actuator.

Losses due to change of area turns during the coil winding end up not being quite large and more or less of the same order of magnitude for all the designs. The only noticeable difference between Designs 5 and 6 is their behaviour during temperature changes. As seen in **(Table 2.5)**, both designs generate the same amount of dipole at the same temperature, but Design 6 performs better in terms of power for decreasing temperatures. For this reason, Design 6 seems the right choice to implement for the air core coil of the magnetorquer.

### 2.3.2 Torquerod design

Torquerod design is similar to the design of air core coils, but there are some critical differences to consider. On one hand, introducing a magnetic core inside the coil substantially increases the generated magnetic moment, reaching values not obtainable with other types of magnetorquer for the same power consumption. The disadvantages of this solution are the increase on mass and dimensions of the system, which are the main constraints during the design, and the difficulty to predict the magnetic behaviour of the core due to non-linearity and hysteresis, which add complexity to their use.

Choosing the material and dimensions of the core is critical to ensure the proper functioning of the torquerod. Both characteristics have a great influence in the efficiency of the system and must be chosen appropriately. However, it must be taken into account that accurate prediction of the torquerod behaviour cannot be reached with mathematical models. Ultimately experimental measures are required to know the real performance of the solution.

Due to their magnetic properties, paramagnetic and ferromagnetic materials may be considered a priori as candidates to use in the core. Paramagnetic materials have the advantage that they do not present residual magnetic dipole moment when the current is switched off, meaning they can be controlled easily by ADCS. However, they have values of permeability that are orders of magnitude lower than ferromagnetic materials, to the point which using a paramagnetic core does not raise enough the generated magnetic moment to justify the increase in mass of the system.

Among ferromagnetic materials, soft types are preferable to use than hard types. Their hysteresis curve can be easily approximated to be linear, and their low values of coercivity and remanence cause that the generated residual dipole is lower than for hard ferromagnetic materials. Moreover, they are easy to magnetize/demagnetize given their narrow hysteresis loops, which is a desirable property if required to degauss the system while on orbit.

The selection of the core material is also influenced by commercial availability. The company Vacuumschmelze offers many products involving magnetic components, including soft magnetic alloys. ULTRAPERM 250 is a Co-Fe alloy with high permeability and low coercivity values, which makes it ideal for

torquerod applications [29]. The most noticeable properties of this alloy are shown in detail in **(Table 2.7)**.

| Properties | ULTRAPERM 250 |
|---|---|
| Saturation of magnetic flux [T] | 0.74 |
| Coercivity [A/cm] | 0.01 - 0.015 |
| Max. Permeability $\mu_{max}$ | 470000 |
| Density [kg/m$^3$] | 8700 |
| Curie Temperature [ºC] | 360 |
| Electr. Resistivity [Ω·m] | 6.00E-07 |

**Table 2.7** Properties of ULTRAPERM 250. [29]

As previously stated, the introduction of the magnetic core drastically modifies the variables involved in the design, most noticeable being the generated magnetic moment and the mass of the system heavily increased. The magnetic moment generated by the torquerod is now contribution of both the solenoid and the magnetization of the core:

$$m = NIA + V_{core}\, M = \pi r^2 (NI + l \cdot M) \qquad \textbf{(2.10)}$$

The contribution of the core depends on its magnetization and its dimensions, so it is intended to maximize these parameters.

An expression relating the field applied by the coil, the total H-field and the magnetization of the core is found when combining equations (1.4), (1.17) and (1.18) respectively.

$$H = \frac{Ni}{l} - N_d\, M \qquad \textbf{(2.11)}$$

Rearranging the last expression it is obtained:

$$M = \frac{\frac{NI}{l} - H}{N_d} \qquad \textbf{(2.12)}$$

where $N_d$ is the demagnetizing factor. From this expression can be seen that in order to maximize M it results of interest to minimize $N_d$ as much as possible. For a cylindrical core, this parameter only depends on the shape of the core [30]:

$$N_d = \frac{4[\ln(\frac{l}{r})-1]}{(\frac{l}{r})^2 - 4\ln(\frac{l}{r})} \quad \textbf{(2.13)}$$

**(Fig. 2.9)** shows the relationship of $N_d$ with the ratio between the length $l$ and the radius $r$ of the core. As it is shown, increasing values of $l/r$ diminish the value of $N_d$, which increase the magnetic effect of the material of the core for a fixed volume.

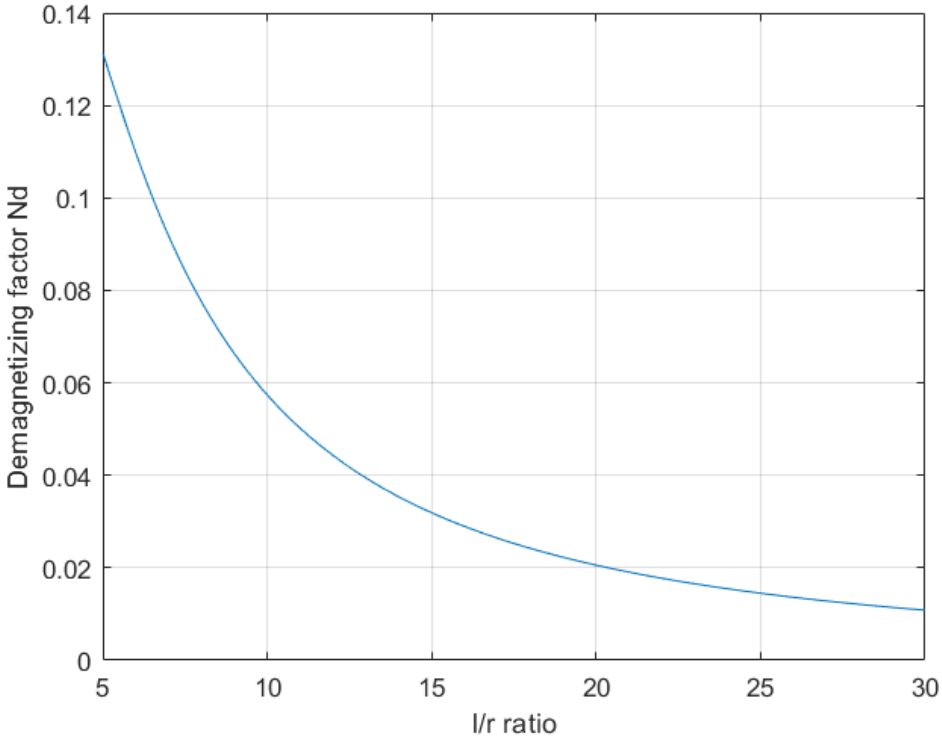


**Fig. 2.9** Demagnetizing factor $N_d$ vs. $l/r$ ratio of the core.

The choice of an appropriate core material allows to assume the linear relationship between $B$ and $H$ given in equation (1.5). On the other hand, the fundamental equation (1.12) that relates $B$, $H$ and $M$ can be used to model the behaviour of the torquerod. Using these expressions with equation (2.11) and expressing permeability in terms of $\mu_0$ one can obtain the following expression for the magnetic field generated by the torquerod:

$$B = \frac{\mu_0 \mu_r N I}{l\,[1+N_d\,(\mu_r-1)]} \quad \textbf{(2.14)}$$

The B-field depends on the properties of the core, the number of turns and the current driven through the coil. This expression does not take into account the

magnetic saturation of the material. Before saturation, the B-field increases rapidly for low increments of current. Once saturation is reached, following increases in $B$ are only due to the influence of the current through the coil. A good design must ensure that the chosen dimensioning of the core allows to reach the desired value of $B$ before or at saturation. Otherwise, the core would be underused.

Finally, making use of equations (2.14), (1.5) and (1.12) in (2.10) it is found an expression for the magnetic moment of the torquerod in terms of the properties of the core and the solenoid:

$$m = \pi r^2 NI \cdot (1 + \frac{(\mu_r - 1)}{1 + (\mu_r - 1) \cdot N_d}) \quad \textbf{(2.13)}$$

There are several key points to discuss in this expression. First of all, it can be observed that the common factor in the equation is the same expression as for the air core coil. Each variable reflects a constraint of the design: the $r^2$ term represents the system dimensions, $N$ can somehow be seen as a representation of the wire mass and $I$ represents the consumed power. Just as with the air core case, $N$ does not have a real impact on the magnetic moment, but serves to trade mass and consumed power during the design.

The first term of the parenthesis represents the contribution of the coil alone, while the second term represents the effect of the magnetic core. This term depends on the permeability of the chosen material and the demagnetizing factor, so it results convenient to design a core with high permeability and a high $l/r$ ratio in order to maximize the obtained magnetic moment.

There are two constraints involved in the dimensioning of the core. First, two torquerods are intended to be placed in the area inside the air core coil. This means that rods must fit within an 80x80 mm square without overlapping. Second, the mass budget limits the weight of the torquerod is 30 g. A margin of 3 g is chosen to be left for the posterior coil design, so 27 g is the mass budget for the core. The constraint also establishes a maximum volume for an Ultraperm core of 3101 $mm^3$, which may be further reduced by the size constraint.

The product of the terms in parenthesis and $r^2$ in equation (2.15) depends on the dimensions of the core for a defined material, so it can be treated as a single variable called geometric parameter $G_p$. **(Fig. 2.10)** shows the dependence of $G_p$ with the dimensions of the core. For the same length, a higher radius means more volume occupied by the core, so $G_p$ increases. For the same radius, a higher length increases the $l/r$ ratio, which also increases $G_p$.

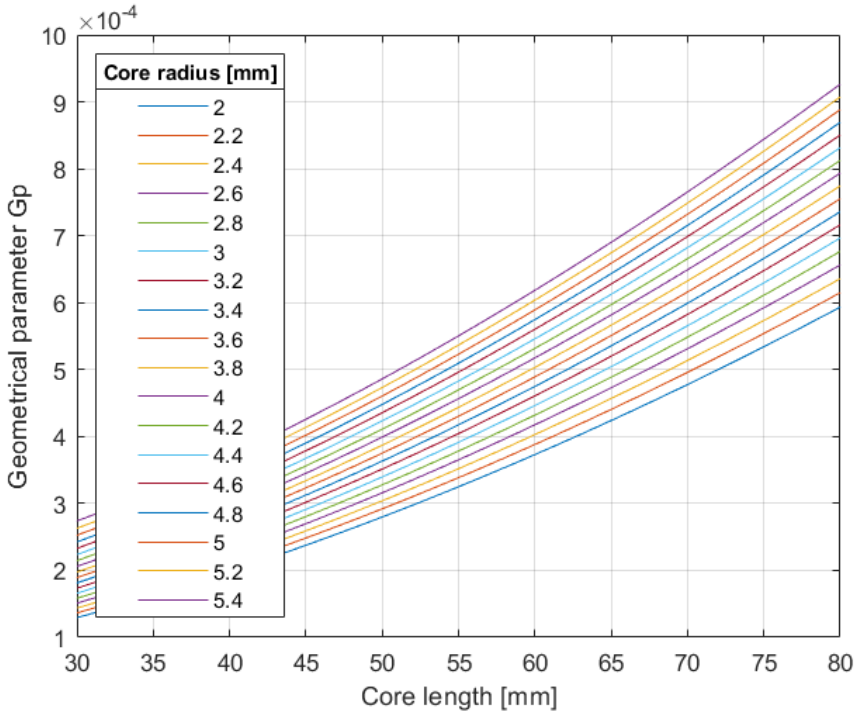


**Fig. 2.10** Geometrical parameter $G_p$ for different values of core radius and length.

The proper selection of the characteristics of the coil also has an important role in the design process. The coil design is quite similar to that of air core, but some differences need to be taken into account. The change of size of the coil means that much less wire is used for torquerods, so voltage supply must be lower respect to the air core coil to ensure design functioning. Torquerods typically operate with a voltage supply of 2.5 V or 3.3 V.

As in the air core case, the generated magnetic moment depends on the chosen wire diameter $a$ for a fixed voltage. However, a thicker wire also increases the power consumption and limits the maximum amount of turns of the coil due to the mass budget.

The appropriate diameter must be chosen to obtain an acceptable magnetic moment while complying with the defined budgets. **(Fig. 2.11)** shows the magnetic moment obtained for different wire diameters and $l/r$ ratios of the core. It is not a bad assumption to choose diameters similar to the ones for the air core case and compare the obtained moment for different $l/r$ ratios.

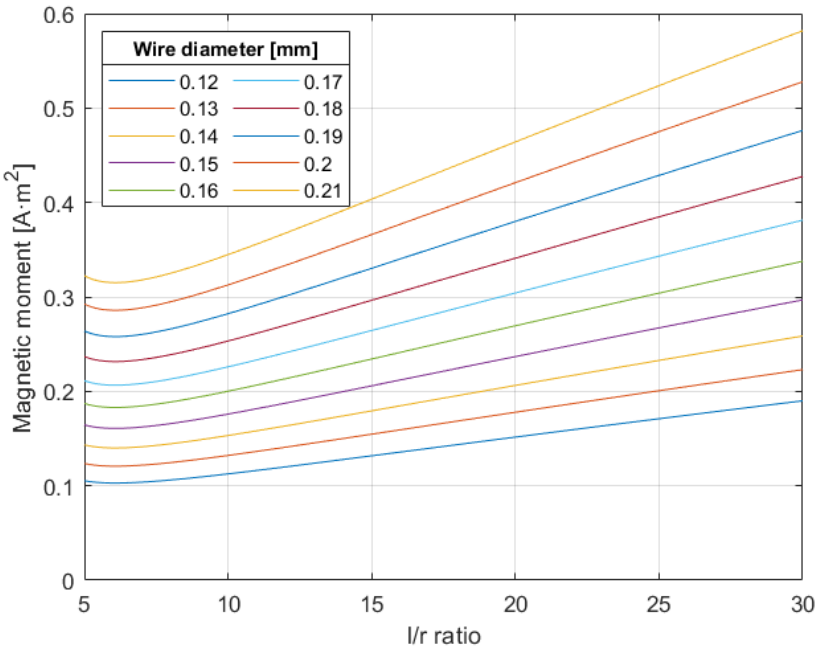


**Fig. 2.11** Generated magnetic moment for different values of wire diameter and $l/r$ ratio ($V$= 2.5 V, $l$= 67 mm).

Once a wire diameter and core dimensions are chosen it is necessary to define the length of the wire in order to determine the power consumption. The number of turns that fit in the coil can be determined in terms of the core length and the wire diameter. Using this, the length and resistance of the wire are also fixed, which allows to compute a power consumption model.

Using only one winding of wire results in an excessive consumption of power. The resistance of the wire is so low that torquerod designs can consume more than 500 mW of power, which is far more than the power budget. A way to solve this is to add more layers of wire to the coil, i.e. add more coil turns above the previous ones once the core is entirely wounded. This method supposed a loss of effective dipole during the air core design given that each new layer increased in area respect to the previous one. However, in the air core torque no more than 3 or 4 layers are needed, so the change in area for each layer can be neglected.

Magnetic moment and power consumption for different values of voltage and $l/r$ ratios are shown below **(Fig. 2.12) (Fig. 2.13)**. These figures consider that 3 layers of wire are wounded around the core.

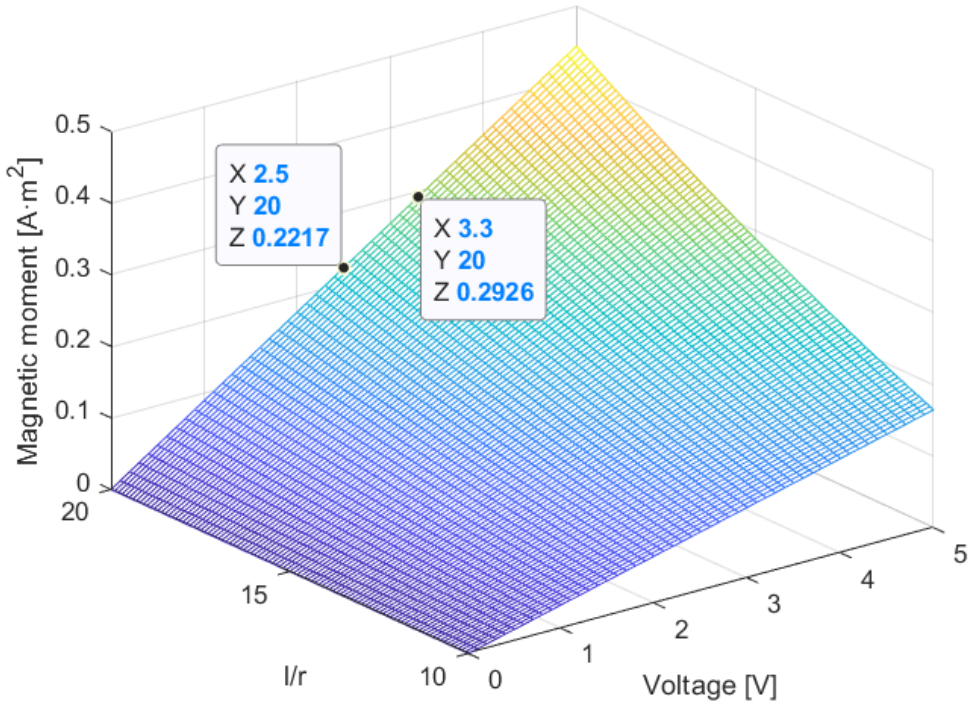


**Fig. 2.12** Magnetic moment obtained for different levels of voltage and $l/r$ ratios ($r$= 3.6 mm, $a$= 0.14 mm).

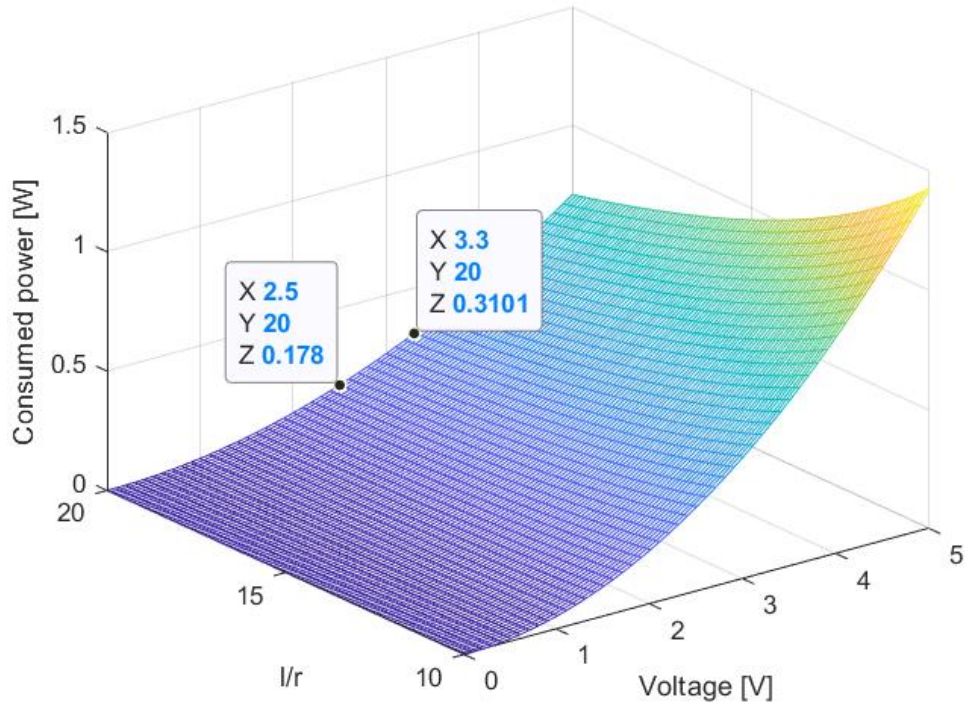


**Fig. 2.13** Power consumption model for different levels of voltage and $l/r$ ratios ($r$= 3.6 mm, $a$= 0.14 mm).

As expected, both magnetic moment and consumed power increase when the voltage is increased. However, for high $l/r$ values the consumed power decreases while the magnetic dipole continues increasing. It appears clear that the shape of the coil is crucial to obtain an efficient design. On the other hand, adding more turns to the coil also helps to reduce the power consumption, as long as the mass budget is not surpassed.

Both figures are obtained considering a wire temperature of 20ºC. Just as in the air core case, magnetic moment and magnetic consumption vary according to the temperature of the device, so an ideal design should also take into account the effects of temperature in the torquerod functioning.

The procedure followed during the torquerod design has been the following: first, the size and shape of the coil are selected given the mass and dimension constraints; second, a wire diameter is chosen and the consumed power, total mass and obtained moment are studied. The objective is to exploit the mass budget and trying to obtain a possible design with as low power consumption as possible for a temperature of 20ºC and a voltage supply of 2.5 V and 3.3 V. Finally, saturation condition and changes of power and magnetic moment due to temperature variations are studied.

| **Parameters** | **Design 1** | **Design 2** |
|---|---|---|
| Core material | Ultraperm 250 | Ultraperm 250 |
| Core radius [mm] | 3.6 | 3.6 |
| Core length [mm] | 68.4 | 70 |
| $l/r$ ratio | 19 | 19.44 |
| Wire material | Copper | Copper |
| Bare wire diameter [mm] | 0.15 | 0.14 |
| Number of turns | 1596 | 1650 |
| Wire length [m] | 36.10 | 37.32 |
| Wire resistance (T=20ºC) [Ω] | 31.66 | 37.58 |
| Total mass [g] | 29.93 | 29.93 |
| Power consumption (V=2.5V, T=20ºC) [mW] | 197.4 | 166.3 |
| Power consumption (V=3.3V, T=20ºC) [mW] | 343.9 | 289.8 |
| Power consumption (V=2.5V, T=-50ºC) [mW] | 271.5 | 228.8 |
| Magnetic dipole moment (V=2.5V, T=20ºC) [A·m$^2$] | 0.2355 | 0.2124 |
| Magnetic dipole moment (V=3.3V, T=20ºC) [A·m$^2$] | - | 0.2804 |

**Table 2.8** Proposed designs for torquerod coil. Values in red do not comply with the requirements of the design.

**(Table 2.8)** presents the obtained results during the torquerod design. Both results are similar, but design 2 makes use of a thinner wire in exchange for a bit larger core. While this reduces the obtained dipole, it also allows to increase the number of turns in order to reduce the consumed power. As a result, design 1 generates a higher magnetic dipole but operates in a smaller temperature interval. On the other hand, design 2 offers more flexibility by being able to operate in conditions of lower temperature despite generating less magnetic moment for the same power supply.

In the end, the decision to choose one or another depends on the operation voltage. For this work, the voltage supply was considered to work at 3.3 V or 5 V, so design 2 is the reasonable choice.

## 2.4 Simulation tests

After the design process is completed, simulations need to be performed in order to test the chosen solution.

The simulations performed in this work have been made using an ADCS simulator developed for the $^{3}$Cat-4 mission in the NanoSat Lab of the UPC – Campus Nord [26] **(Fig. 2.14)**. The satellite of this mission is a 1-Unit CubeSat that uses a gravity boom for passive control and magnetorquers for active control **(Fig. 2.15)**.

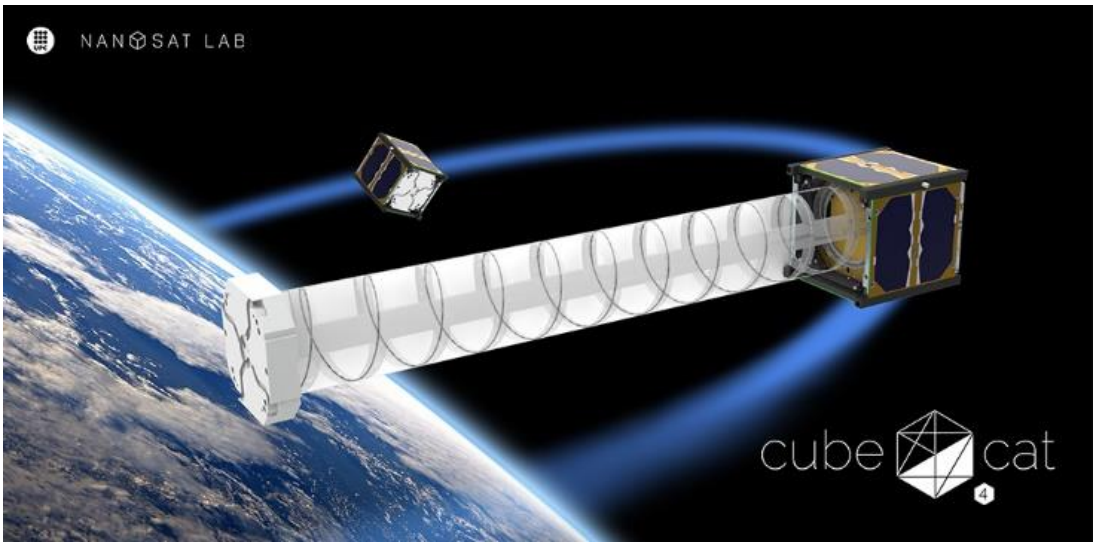


**Fig. 2.14** $^{3}$Cat-4 artist view [26].

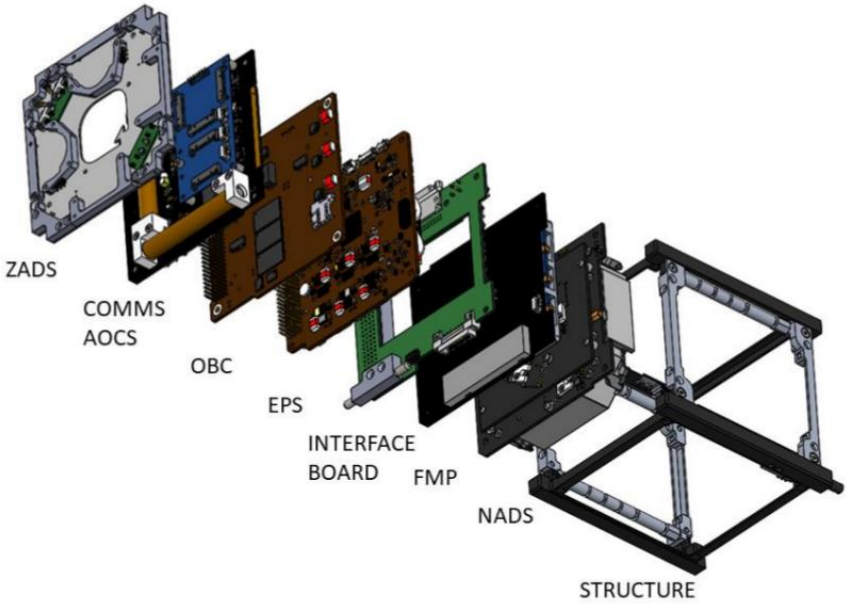


**Fig. 2.15** The different subsystems used by $^{3}$Cat-4. NADS deploys a gravity boom in order to generate a Gravity Gradient. AOCS provides active control by means of magnetic actuation. [26]

The mission intends to provide Earth Observation (EO) from a LEO orbit by means of a RF antenna attached to and deployed with the gravity boom. Due to the altitude of the mission, $^{3}$Cat-4 will be exposed to several types of disturbances that attempt to perturb the attitude of the satellite, including aerodynamic drag, gravity gradient torques, solar radiation pressure and residual magnetic disturbances.

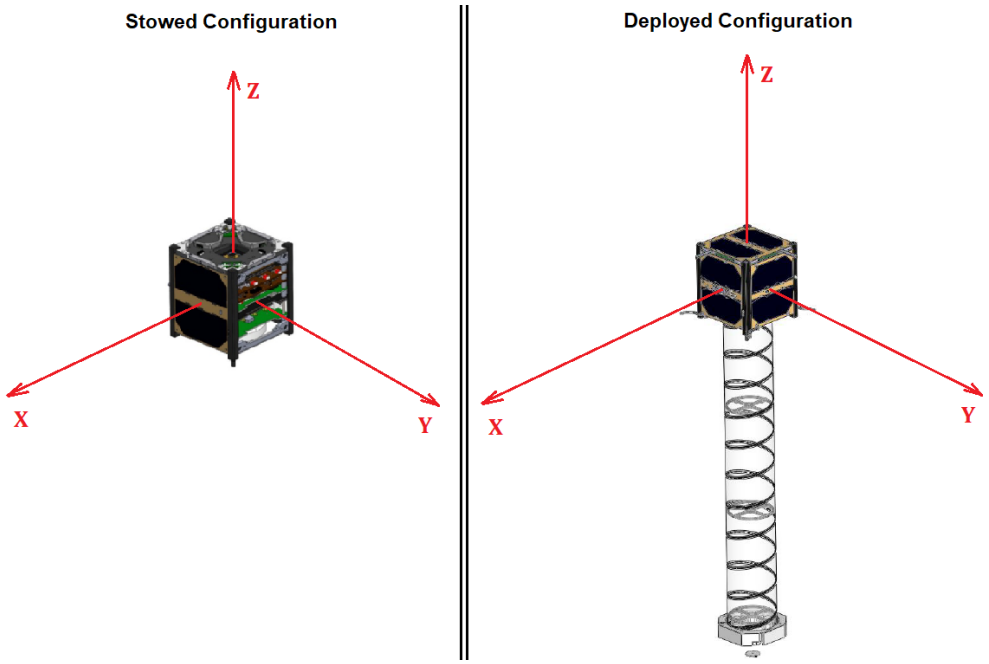


**Fig. 2.16** The two configurations of $^{3}$Cat-4 with respect to the defined Body Reference Frame. [31] [32]

| Parameters | Stowed configuration | Deployed configuration |
|---|---|---|
| Mass [kg] | 1.10 | 1.10 |
| Dimensions | 100 mm x 100 mm x 104.17 mm | 100 mm x 100 mm x 604.2 mm |
| Centre of masses [mm] | (0, 0, 0) mm | (0, 0, -107.6) mm |
| Moment of inertia $I_{xx}$ [kg·m$^2$] | 0.0017 | 0.0521 |
| Moment of inertia $I_{yy}$ [kg·m$^2$] | 0.0017 | 0.0521 |
| Moment of inertia $I_{zz}$ [kg·m$^2$] | 0.0017 | 0.0018 |

**Table 2.9** Parameters of $^3$Cat-4 for the two possible configurations.

The satellite has two possible configurations **(Fig. 2.16) (Table 2.9)**: stowed (gravity boom is retracted) and deployed. The objective of these simulations is to demonstrate that the proposed magnetorquer design is able to control the CubeSat properly in both configurations despite the effect of disturbances.

There are two main control modes available in the simulator, detumbling and nominal. Detumbling mode reduces the angular rate of the three body axes to less than 0.5º/s, but offers no control of the angle deviation. This mode is aimed to be used after orbit insertion. After rotational rates are reduced, nominal mode is activated and the satellite is oriented such as the gravity boom points towards the nadir. The requirements specified for this mode are an angle deviation less than 10º and an angular rate less than 0.5º/s for roll and pitch rotations. No requirements are specified for the z-axis.

The performed simulations are carried over two orbit revolutions and considering the before mentioned disturbance effects. The used body reference frame is defined so the air core coil actuates over the z-axis, i.e. the gravity boom axis, while the torquerods operate over the x and y axes.

The first simulation considers $^3$Cat-4 in stowed configuration and nominal control mode **(Fig. 2.17)**. The initial conditions are set with 0º deviation and 0º/s angular rate for each axis. The aim of this simulation is to check if magnetorquers are capable to provide stability on the satellite on orbit environment.

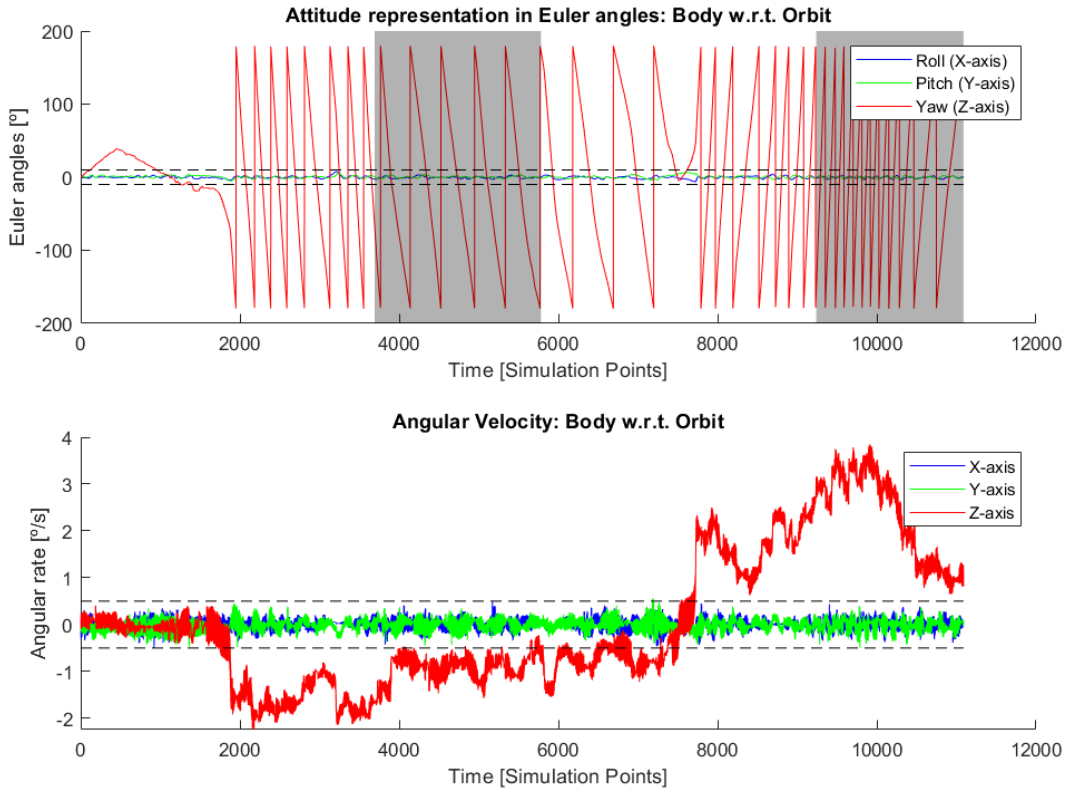


**Fig. 2.17** Attitude performance in stowed configuration and initial conditions set to zero. Dark regions in the first plot correspond to eclipse intervals.

As it can be seen, attitude control is capable to provide stability for roll and pitch and keep the angular rates under the requirement during the entire simulation, giving a 100% pointing percentage. However, the system cannot provide control for the z-axis, which causes yaw angular rate to be unpredictable. This result was expected and does not depend on the proposed solution for magnetorquer, since magnetic actuators are not capable to provide control when aligned with the magnetic field. In order to obtain 3-axis stabilization in $^{3}$Cat-4 additional control actuators such as reaction wheels would be required.

Different perturbations alter the attitude of the satellite **(Fig. 2.18)**. Perturbation effects during this test are mainly due to residual magnetic disturbance torques, which are of the order of 1 μN/m. Gravity gradient, solar radiation pressure and aerodynamic drag disturbance torques have values several orders of magnitude below magnetic disturbance, thus having low contribution on the total disturbance torque.

**(Fig. 2.19)** compares the total disturbance torque with the torque generated by the actuators. The generated torque reaches values one order of magnitude above the total disturbance torque, which is enough to compensate it.

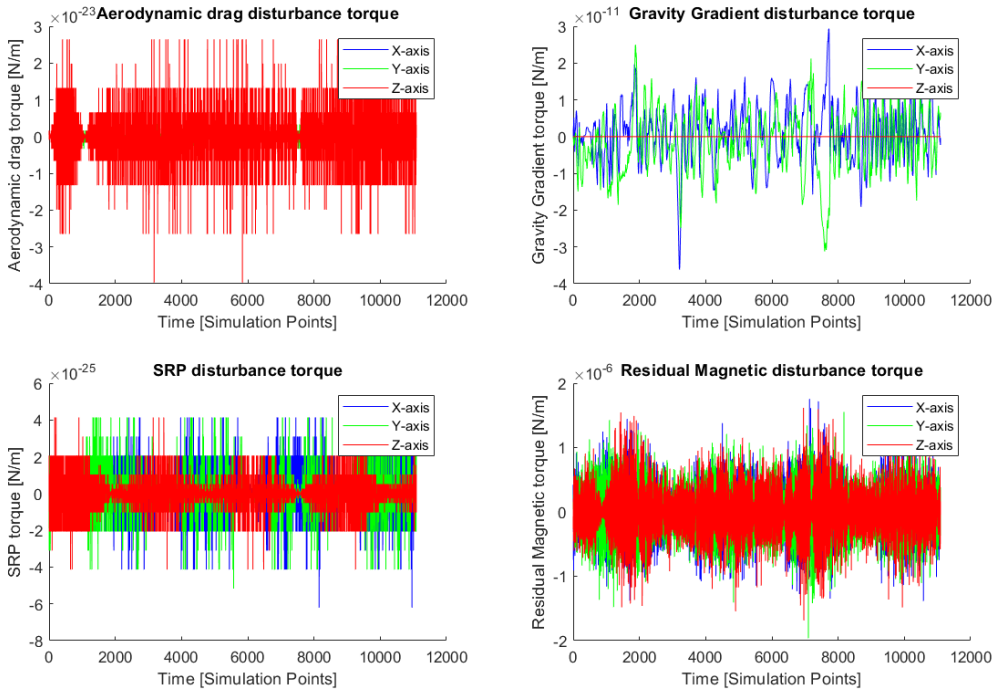


**Fig. 2.18** Disturbance torques affecting the satellite's attitude in stowed configuration.

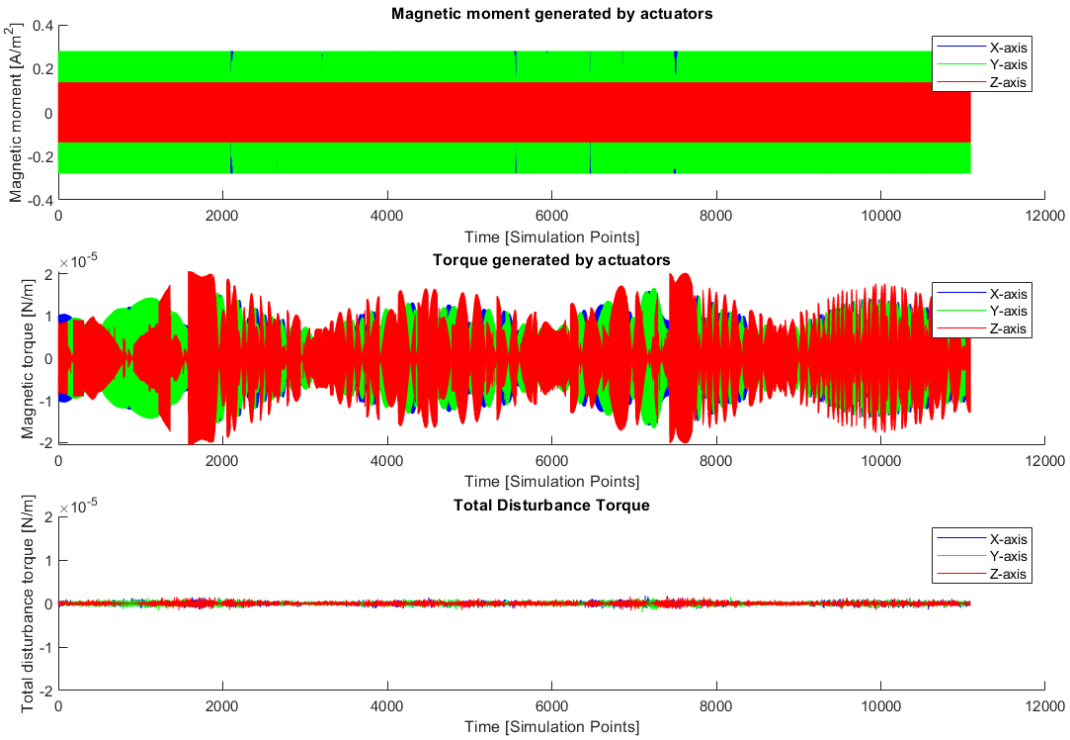


**Fig. 2.19** Magnetic moment and torque generated by actuators and total disturbance torque in stowed configuration and nominal control mode.

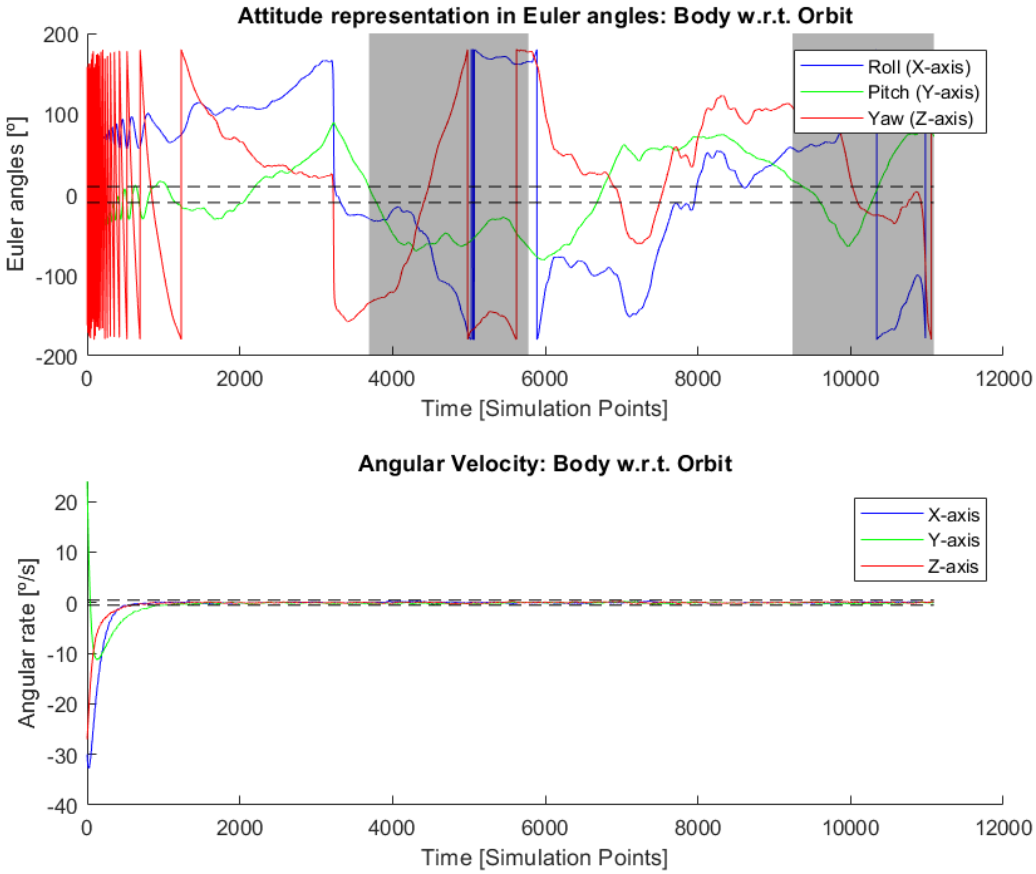


**Fig. 2.20** Performance of detumbling mode in stowed configuration.

**(Fig. 2.20)** shows the performance of the detumbling mode. After orbit insertion, the satellite is capable to dump high initial angular rates (around 30º/s) in the three axes in less than an orbit and keep them under the 0.5º/s threshold. This mode does not offer control over angular deviation though.

Contrary to the previous simulation where actuators work at full power during the entire orbit, in this case magnetic moment is mainly generated during angular rate dumping **(Fig. 2.21)**. Then, the actuator reaches a regime of low consumption that generates magnetic torques of the order of 0.01 µN/m. Despite disturbances being of the same order of magnitude as in the previous case, the satellite keeps low angular rates during the entire simulation.

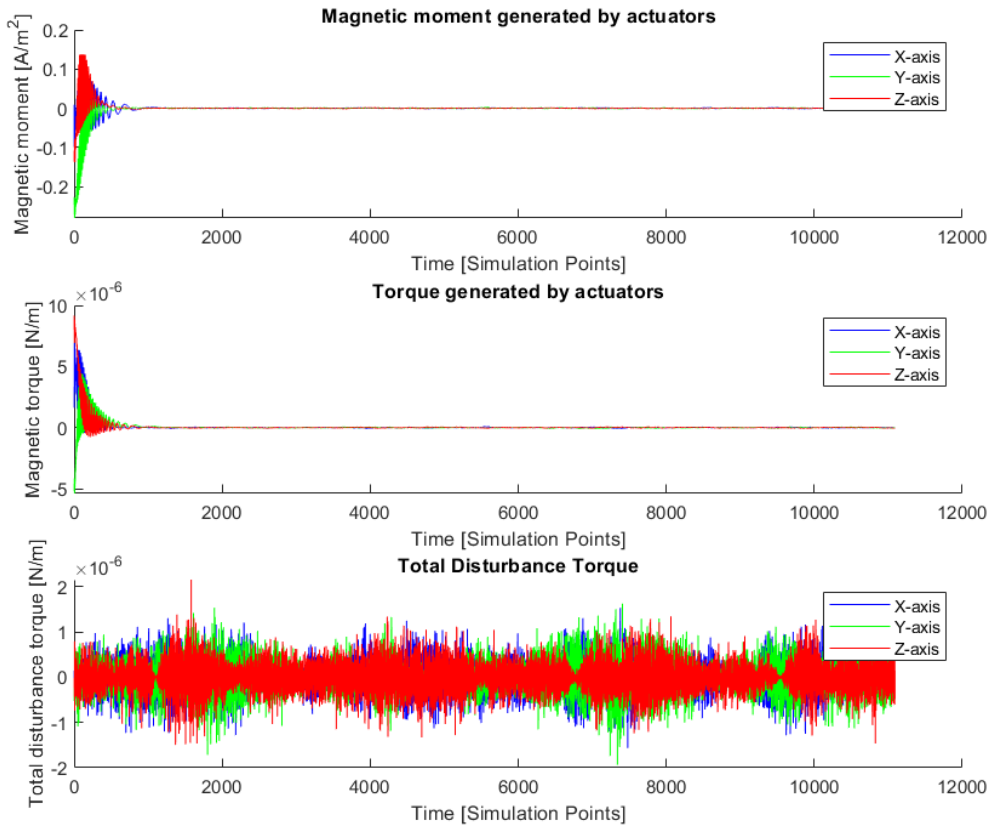


**Fig. 2.21** Magnetic moment and torque generated by actuators and total disturbance torque in stowed configuration.

Once stabilization of the satellite is completed and the z body axis is pointed towards nadir, the gravity boom is deployed. In this configuration, nominal control mode is used to prevent destabilization of the satellite. **(Fig. 2.22)** shows the results of the deployed configuration in nominal mode. As in the first case, rotation around z-axis is still uncontrolled and unpredictable. Control in roll and pitch angle deviation is also a bit less accurate that in the stowed case, exceeding the 10º threshold in few time intervals. However, these cases are punctual; during around 95% of the time the satellite complies with the given constraints.

Due to the change of shape of the satellite, some of the disturbances increase in magnitude, as can be seen in **(Fig. 2.23)**. Aerodynamic drag reaches the order of 1 μN/m for x and y axes, just like residual magnetic disturbance. These two disturbances are the main contribution of the total disturbance over the satellite and the reason for the reduction of accuracy in roll and pitch control. Gravity gradient and solar radiation pressure have also increased in magnitude, but remain having less impact over the satellite's attitude.

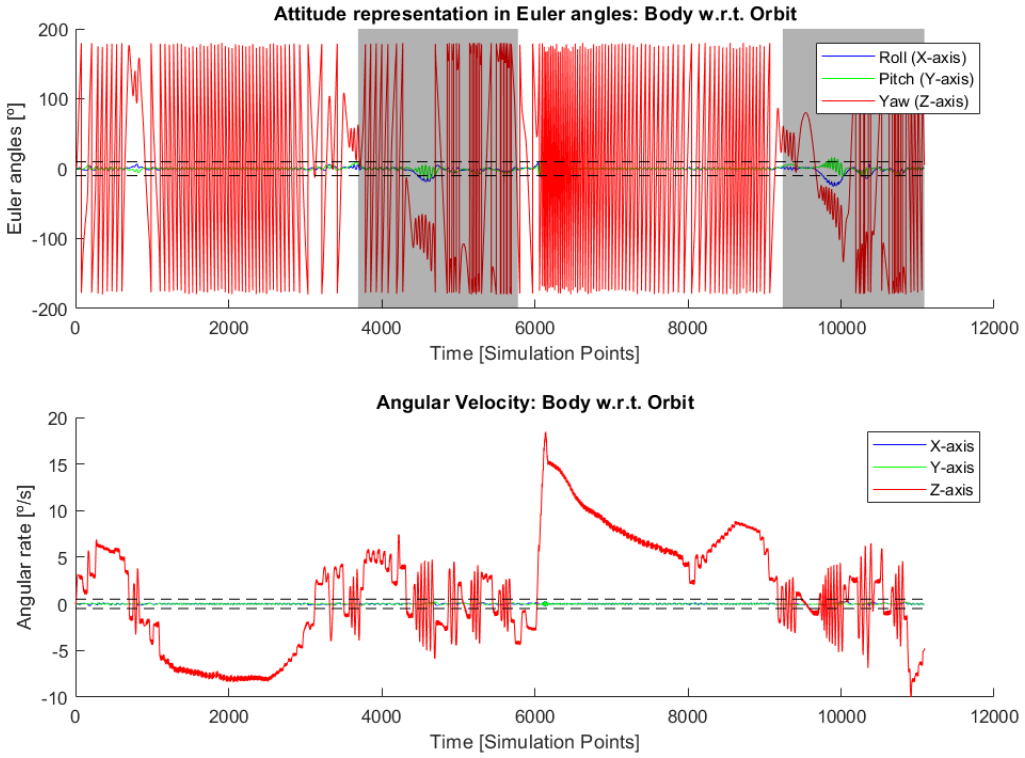


**Fig. 2.22** Attitude performance of [3]Cat-4 in deployed configuration and nominal mode (initial conditions set to zero).

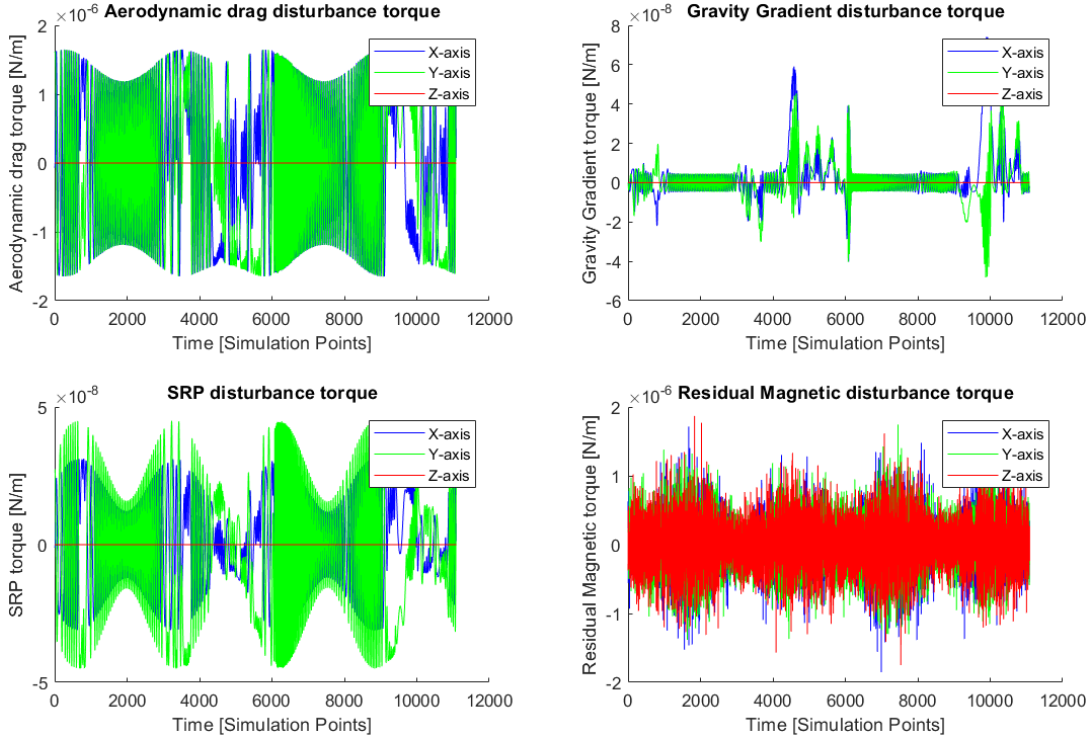


**Fig. 2.23** Disturbance torques affecting the satellite's attitude in deployed configuration.

# CHAPTER 4. CONCLUSIONS AND FUTURE WORK

This project is focused in obtaining the design of a magnetorquer that could be implemented in future 1U CubeSat missions. The design is aimed to obtain a versatile system that could be used in several missions and not only aimed for a specific nanosatellite.

The proposed solution includes an air core coil and two torquerods. The dimensions of the torquerod are chosen so that they are easy to fit in the inside of a CubeSat while also providing an acceptable amount of magnetic moment. Typical temperature changes in LEO orbits are taken into account to ensure operability of the solution within an acceptable temperature margin while complying with the power budget.

The obtained design is tested in an external ADCS Simulator developed for the $^{3}$Cat-4 mission. This satellite also includes a gravity boom for passive control and has two configurations (stowed and deployed) and two control modes (detumbling and nominal). The simulator considers the influence of several disturbance torques in LEO orbits, mainly aerodynamic drag and residual magnetic torques.

Simulations demonstrate that the magnetorquer solution is able to detumble the satellite in stowed configuration after orbit insertion. After that, the system can ensure satellite pointing during a 100% of the time for stowed configuration in nominal mode despite the effect of disturbances mainly caused by residual magnetic torques.

Changes in size and shape of the satellite in deployed configuration increase the effect of aerodynamic drag, which reduces pointing accuracy to 95% of the time.

The results obtained in this work are based on mathematical models and do not entirely validate the proposed design. The performance of a real magnetic actuator is affected by many different variables such as manufacturing errors or environmental factors. In order to truly validate the proposed design it is necessary to build a prototype and test it in orbit conditions.

ADCS tests are usually performed by means of a Helmholtz Cage. This facility is formed by three orthogonal pairs of coils that are capable to generate a uniform magnetic field in the volume within them. In this way, Helmholtz Cages allow 3-axis control of uniform magnetic field found in the volume within the coils.

Calibration of the Helmholtz Cage is required before running every test, in this way Earth’s magnetic field is nullified and a quasi-zero magnetic field is generated inside the measurement volume.

The validation of the prototype must be done coil by coil so as to properly characterize the generated magnetic field of each coil. When current passes through the coil, an amount of magnetic field is generated. Testing for several

values of current and measuring the generated field with a magnetometer placed conveniently inside the cage the magnetic flux density profile of the coil can be obtained. These values are compared with the theoretical ones to ensure that the system behaves as expected.

Typically the performance of the system and the theoretical model will vary according to uncontrollable causes, including external and/or non-uniform magnetic fields or errors during the manufacturing phase. These variations are taking into account by calibrating the system, so that the mathematical model can predict correctly the behaviour of the coils.

# CHAPTER 5. REFERENCES

[1] CubeSat Shop, CubeTorquer and CubeCoil products. (Last access on 19th August 2019): https://www.cubesatshop.com/product/cubetorquer-and-cubecoil/

[2] Fortescue, P., Stark, J., and Swinerd, G., *Spacecraft Systems Engineering*, Wiley-VCH, March 2003.

[3] Nanoavionics, Magnetorquer "SatBus MTQ". (Last access on 19th August 2019): https://n-avionics.com/subsystems/cubesat-magnetorquer-satbus-mtq/

[4] ISIS Products, ISIS Magnetorquer Board. (Last Access on 19th August 2019): https://www.isispace.nl/product/isis-magnetorquer-board/

[5] Miller, D., "Design optimization of the CADRE Magnetorquers", Univerity of Michigan, Ann Arbor (May 2013).

[6] Wertz, J., *Spacecraft Attitude Determination and Control*, Springer, 1980.

[7] Fundamentals of Magnetism. (Last Access on 19th August 2019): http://hyperphysics.phy-astr.gsu.edu/hbase/magnetic/solenoid.html

[8] Gonano, C., Zich, R. and Mussetta, M., "Definition for Polarization *P* and Magnetization *M* Fully Consistent with Maxwell's Equations" (2015).

[9] Wikipedia, Magnetic field. (Last access on 19th August 2019): https://en.wikipedia.org/wiki/Magnetic_field

[10] Wikipedia, Magnetic susceptibility. (Last access on 19th August 2019): https://en.wikipedia.org/wiki/Magnetic_susceptibility

[11] Puig, S., "Modelling Linear and Nonlinear Soft Ferromagnetic Materials" (September 2013).

[12] Wikipedia, Magnetic domains. (Last access on 19th August 2019): https://en.wikipedia.org/wiki/Magnetic_domain

[13] Magnetism. Ferromagnetic materials. (Last access on 19th August 2019): http://ocw.nthu.edu.tw/ocw/upload/124/news/%5b%E9%9B%BB%E5%8B%95%E6%A9%9F%E6%A2%B0L4c%E8%A3%9C%E5%85%85%E6%95%99%E6%9D%90%5dUON_Dr%20Jonathan%20Goss_Ferromagnetism.pdf

[14] NDT Resource Center. The Hysteresis Loop and Magnetic Properties. (Last Access on 19th August 2019): https://www.nde-ed.org/EducationResources/CommunityCollege/MagParticle/Physics/HysteresisLoop.php

[15] Institute for Rock Magnetism. Magnetic Anisotropy. (Last Access on 19th August 2019): http://www.irm.umn.edu/hg2m/hg2m_c/hg2m_c.html

[16] Engineering LibreTexts. Magnetic Hysteresis. (Last access on 19th August 2019): https://eng.libretexts.org/Bookshelves/Materials_Science/Supplemental_Modules_(Materials_Science)/Magnetic_Properties/Magnetic_Hysteresis

[17] Fecioru-Morariu, M., Paduraru, A. and Caltun, O., “The influence of the frequency and waveform on the hysteresis loop of some NiZnCu ferrites”, Al. I. Cuza University, Iasi, Romania (2003).

[18] Szewczyk, R. and Frydrych, P., “Extension of the Jiles-Artherton Model for Modelling the Frequency Dependence of Magnetic Characteristics of Amorphous Alloy Cores for Inductive Components of Electronic Devices”, Warszawa, Poland (2010).

[19] NDT Resource Center. Demagnetization. (Last Access on 19th August 2019): https://www.nde-ed.org/EducationResources/CommunityCollege/MagParticle/Physics/Demagnetization.htm

[20] Magnetic Products and Services, inc., Principles of Magnetism and Stray Currents. (Last access on 19th August 2019): https://gaussbusters.com/resources/articles/principles-of-magnetism/index.html

[21] Cruise, A., Bowles, J., Patrick, T. and Goodall, C., *Principles of Space Instrument Design*, Cambridge Aerospace Series, 2006.

[22] CubeSat Design Specification (CDS), Revision 13. Cal Poly SLO. (Last access on 19th August 2019): https://static1.squarespace.com/static/5418c831e4b0fa4ecac1bacd/t/56e9b62337013b6c063a655a/1458157095454/cds_rev13_final2.pdf

[23] Nanosats Database. (Last access on 19th August 2019): https://www.nanosats.eu/

[24] Space News, “ESA awards five smallsat launcher study contracts”. (Last access on 19th August 2019). https://spacenews.com/esa-awards-five-smallsat-launcher-study-contracts/

[25] Rocket Lab, “Space is open for business, Online”. (Last access on 19th August 2019). https://www.rocketlabusa.com/news/updates/space-is-open-for-business-online/

[26] Universitat Politècnica de Catalunya, NanoSat Lab. 3Cat-4. (Last access on 19th August 2019). https://nanosatlab.upc.edu/en/missions-and-projects/3cat-4

[27] Bellini, N., “Magnetic Actuators for Nanosatellite Attitude Control”. University of Bologna (2014).

[28] Aydinlioglu, A., “Design development and production of electromagnetic coils for Attitude control of a picosatellite”, Aachen (February 2006).

[29] Vacuumschmelze. Soft Magnetic materials and stamped parts, 69 to 82% Nickel-Iron. (Last access on 19th August 2019). https://vacuumschmelze.com/Products/Soft-Magnetic-Materials-and-Stamped-Parts/69-to-82-Nickel-Iron

[30] Fakhari, M., “Design and Manufacturing of a Research Magnetic Torquer Rod”, K.N.Toosi University of Technology, Tehran, Iran (2010).

[31] SlideShare. Small Satellites and Earth Observation. The UPC NanoSat program. (Last access on 26th August 2019). https://www.slideshare.net/adrianocamps/small-satellites-and-earth-observation-the-upc-nanosat-program

[32] European Space Agency. Meet the team: 3Cat-4. (Last access on 26th August 2019). https://www.esa.int/Education/CubeSats_-_Fly_Your_Satellite/Meet_the_team_3Cat-4

# ANNEX 1. MATLAB CODES

This annex gathers all the Matlab codes written and used with the purpose of developing this work.

## airTorquer_coilsDesign_circleCoil.m:

```
clear variables
clf

%Parameters
Pmax=300*10^-3; %Power [W]
Mmax=30*10^-3;  %Mass  [kg]
V=5;

%Inputs
r=40*10^-3;                 %Coil radius [m]
a=(0.12:0.01:0.21)*10^-3;   %Wire diameter [m]
T=20;                       %Temperature [°C]


%Wire material: copper
rho=8.93*10^3;              %Density [kg/m^3]
sigma0=1.55*10^-8;          %Resistivity at T0 [ohm*m]
electrResist0=3.90*10^-3;   %Electrical Resistivity at T0 [1/K]
T0=20;                      %Reference temperature [°C]


sigma=sigma0*(1+electrResist0*(T-T0));
% Plots
N=(100:5:1000);
P=zeros(length(a),length(N));
M=P;
m=P;

for i=1:length(a)
    P(i,:)=V^2*a(i)^2./(sigma*8*r.*N);
    M(i,:)=rho*pi^2*r*a(i)^2.*N/2;
    m(i,:)=(r/2).*sqrt(P(i,:).*M(i,:)/(rho*sigma));
end
figure(1)
plot(N,P);
axis([100 1000 0 1])
grid on
lgd=legend(string(a*10^3));
xlabel('Number of turns');
ylabel('Power consumption (W)');
title(lgd,'Wire diameter (mm)');

figure(2)
plot(N,M);
axis([100 1000 0 0.1])
grid on
legend(string(a*10^3))
lgd=legend(string(a*10^3));
lgd.Location= 'northwest';
xlabel('Number of turns');
ylabel('Wire mass (kg)');
title(lgd,'Wire diameter (mm)');

figure(3)
plot(N,m);
lgd=legend(string(a*10^3));
xlabel('Number of turns');
ylabel('Magnetic dipole moment (A·m^2)');
title(lgd,'Wire diameter (mm)');

%Parameters of the chosen design

% %Design 1 inputs
% t_r=40*10^-3;
% t_N=580;
```

```
% t_a=0.15*10^-3;
% t_M=rho*pi^2*t_r*t_a^2*t_N/2;

% %Design 2 inputs
% t_r=40*10^-3;
% t_N=600;
% t_a=0.16*10^-3;
% t_M=rho*pi^2*t_r*t_a^2*t_N/2;

% % Design 3 inputs
% t_r=40*10^-3;
% t_N=500;
% t_a=0.17*10^-3;
% t_M=rho*pi^2*t_r*t_a^2*t_N/2;

%Design 4 inputs
t_r=40*10^-3;
t_N=580;
t_a=0.17*10^-3;
t_M=rho*pi^2*t_r*t_a^2*t_N/2;

%Power, current, dipole moment vs voltage
t_v=linspace(0,V);
t_i=t_v*t_a^2/(sigma*8*t_r*t_N);
t_p=t_i.*t_v;
t_m=(t_r/2)*sqrt(t_p*t_M/(rho*sigma));

figure(4)
plot(t_v,t_p);
hold on
plot(t_v,t_i);
plot(t_v,t_m);
grid on
xlabel('Voltage supply (V)');
legend('Consumed Power (W)','Current (A)','Magnetic moment (A·m^2)');
hold off
```

## airTorquer_coilsDesign_squareCoil.m:

```
clear variables
clf

%Parameters
Pmax=300*10^-3; %Power [W]
Mmax=30*10^-3;  %Mass  [kg]
V=5;

%Inputs
r=45*10^-3;                     %Coil radius [m]
a=(0.11:0.01:0.21)*10^-3;       %Wire diameter [m]
T=100;                         %Temperature [°C]

%Wire material:

% copper
rho=8.93*10^3;              %Density [kg/m^3]
sigma0=1.55*10^-8;          %Resistivity at T0 [ohm*m]
electrResist0=3.90*10^-3;   %Electrical Resistivity at T0 [1/K]
T0=20;                      %Reference temperature [°C]

% % aluminum
% rho=2.70*10^3;              %Density [kg/m^3]
% sigma0=2.50*10^-8;          %Resistivity at T0 [ohm*m]
% electrResist0=3.90*10^-3;   %Electrical Resistivity at T0 [1/K]
% T0=20;                      %Reference temperature [°C]

sigma=sigma0*(1+electrResist0*(T-T0));
% Plots
N=(100:5:1000);
P=zeros(length(a),length(N));
M=P;
m=P;


for i=1:length(a)
    P(i,:)=V^2*a(i)^2.*(pi/4)./(sigma*8*r*N);
    M(i,:)=rho*pi*2*r*a(i)^2*N;
    m(i,:)=(r/2)*sqrt(P(i,:).*M(i,:)/(rho*sigma));
end
figure(1)
plot(N,P);
axis([100 1000 0 1])
```

```
grid on
lgd=legend(string(a*10^3));
xlabel('Number of turns');
ylabel('Power consumption (W)');
title(lgd,'Wire diameter (mm)');

figure(2)
plot(N,M);
axis([100 1000 0 0.1])
grid on
legend(string(a*10^3))
lgd=legend(string(a*10^3));
lgd.Location= 'northwest';
xlabel('Number of turns');
ylabel('Wire mass (kg)');
title(lgd,'Wire diameter (mm)');

figure(3)
plot(N,m);
lgd=legend(string(a*10^3));
xlabel('Number of turns');
ylabel('Magnetic dipole moment (A·m^2)');
title(lgd,'Wire diameter (mm)');


%Parameters of the chosen design

% %Design 5 inputs
% t_r=45*10^-3;
% t_N=420;
% t_a=0.16*10^-3;
% t_M=rho*2*pi*t_r*t_a^2*t_N;

% %Design 6 inputs
% t_r=45*10^-3;
% t_N=460;
% t_a=0.16*10^-3;
% t_M=rho*2*pi*t_r*t_a^2*t_N;

%Design 7 inputs
t_r=45*10^-3;
t_N=370;
t_a=0.17*10^-3;
t_M=rho*2*pi*t_r*t_a^2*t_N;

% %Design 8 inputs
% t_r=45*10^-3;
% t_N=390;
% t_a=0.17*10^-3;
% t_M=rho*2*pi*t_r*t_a^2*t_N;

% %Design 9 inputs
% t_r=45*10^-3;
% t_N=400;
% t_a=0.17*10^-3;
% t_M=rho*2*pi*t_r*t_a^2*t_N;


%Power, current, dipole moment vs voltage
t_v=linspace(0,V);
t_i=(pi/4)*t_v*t_a^2/(sigma*8*t_r*t_N);
t_p=t_i.*t_v;
t_m=(t_r/2)*sqrt(t_p*t_M/(rho*sigma));

figure(4)
plot(t_v,t_p);
hold on
plot(t_v,t_i);
plot(t_v,t_m);
grid on
xlabel('Voltage supply (V)');
legend('Consumed Power (W)','Current (A)','Magnetic moment (A·m^2)');
hold off

t_m(100)
```

## airTorquer_coilsDesign_wireDiameter.m:

```
clear variables
clf

%Parameters
Pmax=300*10^-3; %Power [W]
Mmax=30*10^-3;  %Mass  [kg]
V=5;
%Inputs
```

```
r=40*10^-3;          %Coil radius [m]
a=linspace(0.09,0.24)*10^-3;    %Wire diameter [m]

%Wire material: copper
rho=8.93*10^3;      %Density [kg/m^3]
sigma=1.55*10^-8;   %Resistivity [ohm*m]

N=350;
P=zeros(1,length(a));
M=P;
m=P;

for i=1:length(a)
    P(i)=V^2*a(i)^2./(sigma*8*r.*N);
    M(i)=rho*pi^2*r*a(i)^2.*N/2;
    m(i)=(r/2).*sqrt(P(i).*M(i)/(rho*sigma));
end

% figure(1)
% plot(N,P);
% lgd=legend(string(a*10^3));
% xlabel('Number of turns');
% ylabel('Power loss (W)');
% title(lgd,'Wire diameter (mm)');
%
% figure(2)
% plot(N,M);
% legend(string(a*10^3))
% lgd=legend(string(a*10^3));
% xlabel('Number of turns');
% ylabel('Mass of the wire (kg)');
% title(lgd,'Wire diameter (mm)');

figure(3)
plot(a*10^3,m);
grid on
% lgd=legend(string(a*10^3));
axis([0.1 0.24 0 0.3]);
xlabel('Wire diameter (mm)');
ylabel('Magnetic dipole moment (A·m^2)');
% title(lgd,'Wire diameter (mm)');

% %Parameters of the chosen design
% %Design 1 inputs
% t_r=40*10^-3;
% t_N=400;
% t_a=0.15*10^-3;
% t_M=rho*pi^2*t_r*t_a^2*t_N/2;
%
% %Design 2 inputs
% t_r=40*10^-3;
% t_N=340;
% t_a=0.14*10^-3;
% t_M=rho*pi^2*t_r*t_a^2*t_N/2;
%
% %Design 3 inputs
% t_r=40*10^-3;
% t_N=440;
% t_a=0.16*10^-3;
% t_M=rho*pi^2*t_r*t_a^2*t_N/2;
%
% %Power, current, dipole moment vs voltage
% t_v=linspace(0,V);
% t_i=t_v*t_a^2/(sigma*8*t_r*t_N);
% t_p=t_i.*t_v;
% t_m=(t_r/2)*sqrt(t_p*t_M/(rho*sigma));
%
% figure(4)
% plot(t_v,t_p);
% hold on
% plot(t_v,t_i);
% plot(t_v,t_m);
% legend('p','i','m');
% hold off
```

## airTorquer_effDipole.m:

```
clear variables;
clf;

%MODELLING CHANGE IN AREA LOOPS

%Input parameters
r=45*10^-3; %Coil radius [m]
d=4*10^-3; %Width of the coil support [m]
a=(0.11:0.01:0.21)*10^-3;    %Wire diameter [m]
```

```
N=(10:5:600);

n_turns=floor(d./a);     %Turns per column (must be integer)

eff_dipole=zeros(length(a),length(N));
for i=1:length(a)
    for j=1:length(N)
        turns=N(j);     %Remaining turns
        column=0;       %Current column of turns (starts at 0)
        real_dipole=0;
        while not(turns==0)
            if turns>=n_turns(i)    %If there are enough turns to complete a column
                if (r-column*a(i))>0
                    real_dipole=real_dipole+n_turns(i)*(r-column*a(i))^2;
                    turns=turns-n_turns(i);
                    column=column+1;
                else
                    fail=true;
                end
            else
                if (r-column*a(i))>0
                    real_dipole=real_dipole+turns*(r-column*a(i))^2;
                    turns=0;
                else
                    fail=true;
                end
            end
        end
        %Ideally, all turns have the same area
        theor_dipole=N(j)*r^2;
        %The efficiency is measured comparing the ideal (theoretical) and real dipoles
        eff_dipole(i,j)=real_dipole/theor_dipole;
    end
end
figure(1)
plot(N,eff_dipole);
grid on;
lgd=legend(string(a*10^3));
lgd.Location= 'southwest';
xlabel('Number of turns');
ylabel('Effective moment/ Ideal moment');
title(lgd,'Wire diameter (mm)');
```

## torquerod_coilsDesign_circleCoil.m:

```
clear variables
clf

%TORQUEROD DESIGN - Coil Design

% Plots of magnetic moment and consumed power vs current and l/r ratio

%Parameters
Pmax=300*10^-3; %Power [W]
Mmax=30*10^-3;  %Mass  [kg]
% V=2.5;

%Inputs
vol=(3107)*10^-9;           % Volume occupied by core [m^3]
l_r=6:0.2:24;               % l/r ratio
in=0:0.1:1.2;               % Current

a=(0.15)*10^-3;             %Wire diameter [m]
T=20;                       %Temperature [°C]

%Wire material: copper
rho=8.93*10^3;              %Density [kg/m^3]
sigma0=1.55*10^-8;          %Resistivity at T0 [ohm*m]
electrResist0=3.90*10^-3;   %Coefficient of Resistivity at T0 [1/K]
T0=20;                      %Reference temperature [°C]

sigma=sigma0*(1+electrResist0*(T-T0));

% Plots
[l_r,in]=meshgrid(l_r,in);
r=(vol./(pi.*l_r)).^(1/3);  %Core radius
l=r.*l_r;                   %Core length
N=l./a;                     %Number of turns (defined by core length)
A=pi.*r.^2;                 %Area covered by turn
L=2*pi.*r.*N;               %Wire length
S=pi*a^2/4;                 %Wire cross section
R=sigma.*L./(S);            %Wire resistance

m=N.*in.*A;                 %Magnetic dipole moment [A*m^2]
P=in.^2.*R;                 %Consumed power [W]

figure(1)
```

```
mesh(in,l_r,m);
xlabel('Current [A]');
ylabel('l/r');
zlabel('Magnetic moment [A·m^2]');

figure(2)
mesh(in,l_r,P);
xlabel('Current [A]');
ylabel('l/r');
zlabel('Consumed power [W]');
```

## torquerod_coreDesign1.m:

```
clear variables
clf

%TORQUEROD DESIGN - Core design (dimensions)

%Plots of volume, mass, Nd and Gp vs length and radius core

r=(3:0.2:5.6)*10^-3;     % Core radius [m]
l=(30:0.5:80)*10^-3;    % Core length [m]

%Wire material: copper
rho_w=8.93*10^3;                %Density [kg/m^3]
% T0=20;                          %Reference temperature [Celsius degrees]
electrResist0=3.90*10^-3;       %Coefficient of Resistivity at T0 [1/K]
sigma0=1.55*10^-8;              %Resistivity at T0 [ohm*m]
% sigma=sigma0*(1+electrResist0*(T-T0));
sigma=sigma0;

% Core material: Ultraperm 250
B_sat=0.74;             % Saturation B-field [T]
H_c=1.0;              % Coercivity H-field [A/m]
mu_r = 4.7*10^5;        % Relative permeability [no units]
xi_core= mu_r-1;        % Magnetic susceptibility [no units]
rho_core=8700;          % Density [kg/m^3]
sigma_core=6*10^-7;     % Electric resistivity [ohm*m]


%Computations

vol_core=NaN(length(r),length(l));
mass_core=vol_core;
Nd=vol_core;
Gp=vol_core;

for i=1:length(r)
    for j=1:length(l)
        vol_core(i,j)=pi*r(i)^2*l(j);               % Core volume [m^3]
        mass_core(i,j)=rho_core*vol_core(i,j);      % Core mass [kg]

        % Demagnetizing factor [no units]
        Nd(i,j)=4*(log(l(j)/r(i))-1)./(((l(j)/r(i))^2)-4.*log(l(j)/r(i)));

        % Geometric parameter of the core (depends on shape and material)
        Gp(i,j)=r(i)^2*(1+xi_core./(1+xi_core.*Nd(i,j)));

    end
end

figure(11)
plot(l*10^3,vol_core*10^9)
grid on
lgd=legend(string(r*10^3));
title(lgd,'Core radius [mm]')
lgd.Location='southwest';
ylabel('Core volume [mm^3]')
xlabel('Core length [mm]')
axis([30 80 0 3200])

figure(12)
plot(l*10^3,mass_core*10^3)
grid on
lgd=legend(string(r*10^3));
title(lgd,'Core radius [mm]')
lgd.Location='southwest';
ylabel('Core mass [g]')
xlabel('Core length [mm]')
axis([30 80 0 30])

figure(13)
plot(l*10^3,Nd)
grid on
lgd=legend(string(r*10^3));
title(lgd,'Core radius [mm]')
lgd.Location='northwest';
```

```
ylabel('Demagnetizing factor Nd')
xlabel('Core length [mm]')

figure(14)
plot(l*10^3,Gp)
grid on
lgd=legend(string(r*10^3));
title(lgd,'Core radius [mm]')
lgd.Location='northwest';
ylabel('Geometrical parameter Gp')
xlabel('Core length [mm]')
```

## torquerod_coreDesign2.m:

```
clear variables;
clf;

%TORQUEROD DESIGN - Dimensions (2)

% Plots of Nd, Gp, magnetic moment and total mass vs l/r ratio and wire
% diameter (Fixed length)

%% Input parameters

Pmax=300*10^-3; % Power [W]
Mmax=30*10^-3;  % Mass  [kg]
V=2.5;          % Voltage supply [V]
T=20;           % Temperature [Celsius degrees]

l=67*10^-3;                 % Core length [m]
a=(0.12:0.01:0.21)*10^-3;   % Wire diameter [m]
l_r=(5:0.1:30);             % Ratio l/r

%% Materials
% Wire material: copper
rho_w=8.93*10^3;                %Density [kg/m^3]
T0=20;                          %Reference temperature [Celsius degrees]
electrResist0=3.90*10^-3;       %Coefficient of Resistivity at T0 [1/K]
sigma0=1.55*10^-8;              %Resistivity at T0 [ohm*m]
sigma=sigma0*(1+electrResist0*(T-T0));

% Core material: Ultraperm 250
B_sat=0.74;             % Saturation B-field [T]
H_c=1.0;              % Coercivity H-field [A/m]
mu_r = 4.7*10^5;        % Relative permeability [no units]
xi_core= mu_r-1;        % Magnetic susceptibility [no units]
rho_core=8700;          % Density [kg/m^3]
sigma_core=6*10^-7;     % Electric resistivity [ohm*m]

%% Computations

W_res=4.*sigma./(pi*a.^2);          % Wire specific resistance (sigma/wire section) [ohm/m]
r= l./l_r;                          % Coil radius [m]

k=1;
N=k*l./a;                           % Number of turns

Nd=4*(log(l_r)-1)./((l_r.^2)-4.*log(l_r));  % Demagnetizing factor [no units]
Gp_r=r.*(1+xi_core./(1+xi_core.*Nd));       % Geometric parameter of the core (depends on shape and
material)

m=NaN(length(W_res),length(Gp_r));   % Magnetic dipole moment depending on Gp and a
M=m;
for i=1:length(W_res)
    for j=1:length(Gp_r)
        m(i,j)=Gp_r(j)*V/(2*W_res(i));
        M(i,j)=pi*l*(pi*N(i)*rho_w*a(i)^2/(2*l_r(j))+rho_core*r(j)^2);
    end
end


%% Plots
figure(21)
plot(l_r,Nd);
grid on
ylabel('Demagnetizing factor Nd')
xlabel('l/r ratio')

figure(22)
plot(l_r,Gp_r);
grid on
ylabel('Geometrical parameter Gp/r')
xlabel('l/r ratio')

figure(23)
plot(l_r,m)
grid on
axis([5 30 0 0.6])
```

```
lgd=legend(string(a*10^3));
title(lgd,'Wire diameter [mm]')
lgd.NumColumns=2;
lgd.Location='northwest';
ylabel('Magnetic moment [A·m^2]')
xlabel('l/r ratio')

figure(24)
plot(l_r,M)
grid on
lgd=legend(string(a*10^3));
title(lgd,'Wire diameter [mm]')
ylabel('Total mass [kg]')
xlabel('l/r ratio')
```

## torquerod_testDesign.m:

```
clear variables
clf

%Torquerod - Test design

%Plots to check the performance of a design (magnetic moment, power
%consumption and mass)

%% Parameters

mu_0=4*pi*10^-7;    %Permeability of free space [N/A^2]
T=-50;               %Temperature [Celsius degrees]

%Wire material: copper
rho_w=8.93*10^3;                %Density [kg/m^3]
T0=20;                          %Reference temperature [Celsius degrees]
electrResist0=3.90*10^-3;       %Coefficient of Resistivity at T0 [1/K]
sigma0=1.55*10^-8;              %Resistivity at T0 [ohm*m]
sigma=sigma0*(1+electrResist0*(T-T0));
% sigma=sigma0;

% Core material: Ultraperm 250
B_sat=0.74;             % Saturation B-field [T]
H_c=1.0;              % Coercivity H-field [A/m]
mu_r = 4.7*10^5;        % Relative permeability [no units]
xi_core= mu_r-1;        % Magnetic susceptibility [no units]
rho_core=8700;          % Density [kg/m^3]
sigma_core=6*10^-7;     % Electric resistivity [ohm*m]

%% Test design

t_r=3.6*10^-3;                      % Core radius [m]
% t_l=68.5*10^-3;

t_V=0:0.1:5;                        % Voltage supply [V]
% t_l_r=10:0.1:20;                    % l/r ratio
t_l_r=10:0.1:19.44;
t_l_r(:,95)=70/3.6;

[t_l_r,t_V]=meshgrid(t_l_r,t_V);
t_l=t_l_r.*t_r;                     % Core length [m]

t_a=0.14*10^-3;                     % Wire diameter [m]


t_k=3.3;
t_N=t_k*floor(t_l./t_a);            % Number of turns
t_N(:,95)=1650;

t_L=2*pi*t_r.*t_N;                  % Wire length [m]
t_R=sigma.*4.*t_L./(pi*t_a^2);      % Wire resistance [ohm]
t_in=t_V./t_R;                      % Current applied [A]

t_Nd=4.*(log(t_l_r)-1)./((t_l_r.^2)-4.*log(t_l_r));
t_m=pi*t_r^2.*t_N.*t_in.*(1+xi_core./(1+xi_core.*t_Nd));
t_P=t_in.^2.*t_R;
t_M=pi.*t_l.*(pi.*t_N.*t_a.^2.*rho_w./(2.*t_l_r)+rho_core.*t_r.^2);

figure(31)
mesh(t_V,t_l_r,t_m);
xlabel('Voltage [V]');
ylabel('l/r');
zlabel('Magnetic moment [A·m^2]');

figure(32)
mesh(t_V,t_l_r,t_P);
xlabel('Voltage [V]');
ylabel('l/r');
zlabel('Consumed power [W]');

figure(33)
```

```
plot(t_l_r(1,:),t_M(1,:)*10^3);
xlabel('l/r');
ylabel('Mass [g]');
grid on;

%%%%%%%%%%%%%%%%%%%%%%%%%%%%%%%%%%%%%%%%
%Check dimsensions of the system
%%%%%%%%%%%%%%%%%%%%%%%%%%%%%%%%%%%%%%%%

%Two torquerods must fit in an 80x80 mm square
dim_r=3.6; %mm
dim_l=70; %mm

barra1=[dim_r*2 dim_l];
barra2=[80-dim_l 80-2*dim_r];

%Vector joining the 2 closest points. If both components are negative, the
%system overlaps
resta=barra2-barra1;
%Distance between the 2 closest points
dis=sqrt((barra1(1)-barra2(1))^2+(barra1(2)-barra2(2))^2);

disp(resta);disp(dis);
```

## torquerod_testDesign_saturation.m:

```
clear variables
clf

%Torquerod - Test design - Saturation

% Plots of magnetic moment and B-Field vs wire diameter

%% Parameters
mu_0=4*pi*10^-7;            %Permeability of free space [N/A^2]
T=20;                       %Temperature [Celsius degrees]

%Wire material: copper
rho_w=8.93*10^3;                %Density [kg/m^3]
T0=20;                          %Reference temperature [Celsius degrees]
electrResist0=3.90*10^-3;       %Electrical Resistivity at T0 [1/K]
sigma0=1.55*10^-8;              %Resistivity at T0 [ohm*m]
sigma=sigma0*(1+electrResist0*(T-T0));
% sigma=sigma0;

% Core material: Ultraperm 250
B_sat=0.74;             % Saturation B-field [T]
H_c=1.0;              % Coercivity H-field [A/m]
mu_r = 4.7*10^5;        % Relative permeability [no units]
xi_core= mu_r-1;        % Magnetic susceptibility [no units]
rho_core=8700;          % Density [kg/m^3]
sigma_core=6*10^-7;     % Electric resistivity [ohm*m]

%% Saturation test

t_r=3.6*10^-3;                  % Core radius [m]
% t_l_r=19;                       % l/r ratio
% t_l=t_l_r*t_r;                  % Core length [m]
t_l=70*10^-3;
t_l_r=t_l/t_r;

t_N=1600;                       % Number of turns
t_V=3.3;                        % Voltage [V]
t_a=(0.10:0.002:0.30)*10^-3;    % Wire diameter [m]

t_L=2*pi.*t_r.*t_N;                 % Wire length [m]
t_R=sigma.*4.*t_L./(pi.*t_a.^2);    % Wire resistance [ohm]

t_Nd=4.*(log(t_l_r)-1)./((t_l_r.^2)-4.*log(t_l_r)); % Demagnetizing factor

t_B=mu_0*mu_r.*t_N.*t_V./(t_R.*t_l.*(1+t_Nd.*(mu_r-1)));
t_m=pi.*t_r.^2.*(t_N.*t_V./t_R+t_l.*t_B.*(mu_r-1)./(mu_0.*mu_r));

%Plots
figure(41)
plot(t_a*10^3,t_B)
grid on
xlabel('Wire diameter [mm]')
ylabel('B-field [T]')

figure(42)
plot(t_a*10^3,t_m)
grid on
xlabel('Wire diameter [mm]')
ylabel('Magnetic moment [A·m^2]')
```